

# **Quantifying the Changes in Material Characteristics during Dilute Phase Pneumatic Conveying**

## **Process and Food Technology**

Nathan Pantjadarma

17007194

Company Supervisors: Johan Groen, Sean Xu

School Supervisors: Caroline Mok, Mark Leemhuis

Date: Sunday, August 1, 2021

## **Abstract**

Pneumatic conveying is a transportation method for particulate materials commonly employed in industrial processes. Specifically, dilute phase pneumatic conveying, characterized by high gas velocities, low solid to air ratio, and low pressure drop, is utilized. In this report, three types of materials were pneumatically conveyed: lignin particles (fragile material), high fat cocoa powder (heat sensitive material), and rubber particles (highly elastic material). The experiments were done in three distinct setups based on pipe diameter and pipe orientation: 12 mm horizontal, 22 mm horizontal, and 22 mm vertical. Gas velocity and bend number were two other variables that were used in the experimental design – extremes were used: high velocity, low velocity, three bends, and nine bends. The breakage of lignin particles was measured with sieving. Then the PSD was determined with laser diffraction. Cocoa powder yield was measured by weighing. Then the PSD was determined with laser diffraction. Finally, the circularity, convexity, and elongation of rubber particles were determined before and after pneumatic conveying to determine whether there were changes in shape distribution. Particle imaging was used for this.

## Contents

1. Introduction .....	5
1.1. Background .....	5
1.2. Aim & Objectives .....	6
2. Theoretical Background.....	7
2.1. Pneumatic conveying.....	7
2.1.1. What is pneumatic conveying?.....	7
2.1.2. Dilute phase vs. Dense phase .....	7
2.1.3. Positive pressure vs. negative pressure (vacuum).....	8
2.1.4. Saltation Velocity & Choking Velocity .....	8
2.2. Equipment and Material.....	9
2.3. Materials .....	10
2.3.1. Friable Materials.....	10
2.3.2. Heat Sensitive Materials (Agglomeration) .....	12
2.3.3. Highly Elastic Materials (Elongation) .....	12
2.4. Analytical Methods.....	13
2.4.1. Laser Diffraction Spectrometry .....	13
2.4.2. Particle Imaging Microscopy .....	15
2.4.3. Sieving .....	17
3. Methodology .....	17
3.1. Pneumatic Conveying System Design.....	17
3.2. Determination of the Saltation Velocity .....	18
3.3. Extra Hardware.....	18
3.4. Experimental Procedures.....	19
3.4.1. Lignin.....	19
3.4.2. Cocoa powder.....	19
3.4.3. Rubber particles.....	19
3.4.4. Experiments executed.....	20
4. Results and Discussion .....	20
4.1. Lignin.....	20
4.1.1. 12mm Horizontal breakage percentage .....	21
4.1.2. 22mm Horizontal breakage percentage .....	23
4.1.3. 22mm Vertical breakage percentage.....	25
4.1.4. Laser diffraction results of lignin from 12H, 22H, and 22V .....	28
4.2. Cocoa Powder .....	30
4.2.1. Cocoa Powder at Elevated Temperature .....	31

4.2.2.	12 mm Horizontal Cocoa Yield .....	32
4.2.3.	22 mm Horizontal Cocoa Yield .....	33
4.2.4.	22 mm Vertical Cocoa Yield.....	35
4.2.5.	Laser diffraction results of cocoa from 12H, 22H, and 22V .....	37
4.3.	Rubber Particles .....	40
4.3.1.	Original/As-received rubber particles.....	40
4.3.2.	12 mm Horizontal Setup (Original vs. Extreme vs. Mild) .....	42
4.3.3.	22 mm Horizontal Setup (Original vs. Extreme vs. Mild) .....	45
4.3.4.	22 mm Vertical Setup (Original vs. Extreme vs. Mild).....	47
4.3.5.	Comparison of All Setups (Original vs. Extreme Vs. Mild).....	49
5.	Conclusions.....	51
6.	Recommendations .....	52
	References.....	53
	Appendix .....	56



## 1. Introduction

### 1.1. Background

Pneumatic conveying (PC) is a common transportation technique employed in the processing of solid materials, normally in the form of powders or granulates, using gas (Rhodes, 1998). In pneumatic conveying, there are generally two ways granulated and powdered materials can be conveyed. These are dilute phase and dense phase. In dilute phase, the gas velocity is high, the ratio of solids to air is low, and there is a low pressure drop. The material travels suspended in the air. In the dense phase, the gas velocity is low, the ratio of solids to air is high and there is high pressure drop. The materials when conveyed in dense phase move as chunks or slugs within the piping system. In the processing world, dilute phase pneumatic conveying is very common. The high velocities in dilute phase PC are able to cause changes to either the powder/granulates or the pneumatic conveying system itself due to the increased impact force between the conveyed material and the piping system (bends and pipe wall), or even particle-particle impact.

The orientation of the PC system (horizontal vs. vertical) is important to keep in mind due to its implications on the gas velocity. In a horizontal pipe, the minimum gas velocity to keep the solids suspended in the air stream is known as the saltation velocity. Anything slower than this and the solids will "salt" out of the air stream onto the bottom of the pipe. Of course, the pipe diameter will influence this velocity i.e. larger pipe diameter will need a higher gas flowrate to maintain saltation velocity compared to a pipe with a small diameter. In a vertical pipe, a similar, minimum gas velocity is utilized – the choking velocity. In the case of a vertical pipe, when the choking velocity is not achieved, the solids will begin to fall back on themselves, creating a plug and increasing pressure drop. As a result, it may not be possible for this plug to be re-fluidized (“Choking Velocity in Pneumatic Transport”).

In the PC system, there will be a presence of elbows or bends. They change the direction of the solid flow. There are many types of bends, and each bend has a particular application; each one comes with its own advantages and disadvantages. Generally, the bend types can be divided into two groups: standard bends and specialty bends. For the standard elbows, there are long standard bends, which have a centerline that is eight or more times the pipe diameter and there are short standard bends, which have a centerline that is three to five times the diameter. Standard short elbows are readily available in a variety of sizes, materials, and angles. There is no change in diameter, low pressure losses, and are cheap. Contrarily, when these standard short radius bends are used, fragile materials break or get smoothened out when they impact the bend wall and sensitive materials can smear and build up on the inside of the bends. They would also need surface treatment if abrasive materials are handled (Wagner, 2007). Due to these occurrences that take place, the standard short bend is used in this project.

Depending on the materials being conveyed, there will be different effects on either those materials or the piping system. Assuming that the gas velocity and the system structure e.g. number of bends are kept constant, then the only variable left is the characteristics of each type of material. In industry, many different types of materials can be conveyed. The materials that commonly cause problems in industrial practice are fragile materials, heat sensitive materials, elastic materials, and abrasive materials. In this project, only the first three materials types of materials are used. They are lignin particles, cocoa powder, and rubber granulates. What happens to these are:

- 1) Fragile materials (Lignin): Easily break, quality issue with products, dust formation resulting in an explosion hazard at a certain dustiness level. Although this also depends on whether the dust cloud can be ignited. With an abundance of fines, filters can also clog easier. Exposure to dust can lead to the irritation of eyes, skin, and lungs, and over time can result in critical lung diseases (“Dust Hazards in Mining”).
- 2) Heat sensitive materials (cocoa powder): Agglomerate, resulting in increasingly clogged pipes/bends which can cause quality issues/spoilage if not checked (for foods) and/or temporary shutdown of production for cleaning. The main point here is pipeline blockage.

- 3) Elastic materials (rubber particles): Stretches easily, resulting in quality changes. In extreme cases, angel hairs or streamers can appear (for polymeric materials). This lowers product quality and can reduce production throughput e.g. the elongated angel hairs could get stuck at the elbows or bends.

Based on this problem, the following **key question** was created: *To what extent does lignin powder break, cocoa powder agglomerate, and rubber particles deform under a given flowrate, certain number of bends, pipe diameter, and orientation during pneumatic conveying?*

The volumetric flowrate of gas and pipe diameter are important variables because the flowrate is what causes the materials to be conveyed in the first place. The gas velocity is a function of the flowrate and the pipe diameter and it is well documented that higher gas velocities will increase the impact force between the solids and bend wall and exacerbate the effects on the different solids (Verma et al., 2018; Mills et al., 2004).

To provide a conclusion for this question, the project began with some literature research in order to gain a better understanding of pneumatic conveying. Next, a lab-scale setup was built and different types of powders/granulates were obtained. The materials were pneumatically conveyed through the PC system and recollected at the other end. These samples were then analyzed using different techniques such as laser diffraction and particle imaging based on the material's most prominent characteristics in order to conclude on the potential changes caused by conveying process.

The theoretical background starts in chapter 2 where pneumatic conveying and the aspects of it are described. Chapter 3 is about how the experiments and analysis of the materials were executed. The results in chapter 4 display the measured changes experienced by the particles. In chapter 5, the results are discussed and concluded and further recommendations are given in chapter 6.

## 1.2. Aim & Objectives

This project covers several different aspects of pneumatic conveying and the variables studied were the different solids used, pipe diameter, gas velocity, number of bends, and orientation of the system (horizontal vs. vertical). The main aim of this project was to simulate industrial dilute phase pneumatic conveying on a lab-scale and see how the aforementioned variables can influence the solid materials. There are several objectives needed to do this:

- Present how a pneumatic conveying system works and explain the main factors that differentiate one PC system from another.
- Build a leak-tight, horizontal PC setup, with particular pipe diameter.
- Build a leak-tight, vertical PC setup, with particular pipe diameter.
- Execute pneumatic conveying experiments with different materials, different setups, different velocities, and different number of bends.
- Identify and quantify the production of fines and changes in the particle size when lignin powder breaks using a size fraction mass difference (sieving) and laser diffraction.
- Identify and quantify the agglomeration of cocoa powder after PC using laser diffraction.
- Identify and quantify the change in rubber particle morphology after PC using particle imaging analysis.
- Identify and quantify the erosion rate of the PC system bends using SEM EDX on the conveyed material after PC.

## 2. Theoretical Background

### 2.1. Pneumatic conveying

#### 2.1.1. What is pneumatic conveying?

Pneumatic conveying is a method of transportation of particulate solids using gas through a pipeline. Another term that is commonly used is pneumatic transport (Rhodes, 2008). The first recorded use of a pneumatic conveyor was in England in 1883. It was used to transfer grain with a blower (Wilms, 2002). Nowadays, it is extensively used in the chemical, food, and cement industries, as well as in thermal plants to transport pulverized coal (Huber & Sommerfeld, 1998). It is also a process that is frequently applied in petrochemical industries due to its flexibility, security in the transportation of high-valued products, ease of control, and low maintenance costs (Barbosa & Seleghim, 2003). According to Purutyan et al. (2001), the two main advantages of pneumatic conveying as a transportation system are:

- 1) Cleanliness and containment – A properly built PC setup can be virtually dust free.
- 2) Low contamination – Having a sealed system greatly reduces the contamination level and chances of contact with moving mechanical components.

As explained by Hall (2012), pneumatic conveying systems are comprised of four different parts:

- 1) Prime mover: The prime mover is the main piece of equipment used to move the gas stream. They can be compressors, fans, blowers, and vacuum pumps.
- 2) Feed: Feed is the material inlet point of the conveying system where it is introduced to the gas stream by vacuum or specially designed valves, pumps, or blow vessels.
- 3) Conveying piping: The part of the PC system through which the material is transported. Here, the pipe diameter, length, slopes, and the amount and types of bends are taken into consideration.
- 4) Disengagement: The last part of the PC system where the solids are separated from the gas stream by cyclone separators or fabric filters. The solids are recollected here and the gas is either disposed of or used again (closed loop PC design).

Verma et al. (2018) reported something similar – they reported that a typical pneumatic conveying system consists of a source of compressed air, a feeding device, conveying pipeline, and a receiver. The source of compressed air would be a positive displacement pump. This kind of pump can also be used in a negative pressure system.

#### 2.1.2. Dilute phase vs. Dense phase

In general, there are two types of pneumatic conveying methods. They are called dilute phase and dense phase pneumatic conveying. In dilute phase, particles are conveyed in a suspension. Therefore, gas velocities are high (usually greater than 20 m/s), solids concentration is low, (less than 1% volume), and there is low pressure drop per unit length of the pipeline. When the gas velocity is made relatively low (usually 1 to 5 m/s), the particles drop out of suspension and flow in dunes or as a pulsating bed. This is known as dense phase pneumatic conveying. Here, the solids concentration is high (30% volume) and the pressure drop per unit length of the pipeline is also high. The particles in dense phase pneumatic conveying are not fully suspended, so there are a lot of particle-particle interactions. Due to the low gas velocities and relatively gentle movement of the solids, dense phase is used for abrasive and friable materials, as product degradation and erosive wear are avoided (Rhodes, 1998; Alkassar et al., 2020). Dilute phase conveying is more versatile in use and therefore it is the typical PC technique (Ortega-Rivas, 2017).

### 2.1.3. Positive pressure vs. negative pressure (vacuum)

In industry, besides pneumatic conveying in dilute phase and dense phase, there is also the choice of using positive pressure or negative pressure (vacuum). Positive pressure is typically used when the bulk material is conveyed from a single source to multiple destinations. In the pneumatic conveying process, a positive displacement blower is placed prior to the material inlet. Positive pressure systems are characterized by the medium to long distances through which they can convey material (around 50-150 m) (“Solutions for pneumatic Conveying”) and high throughputs (Nowak, 2017).

Negative pressure is used typically when material is conveyed from multiple sources to a single point or multiple points. If the material is conveyed to multiple destinations, then each collector or receiving hopper should have its own filter and partial vacuum capability – that could become costly (Bhatia, 2021). Another point to take note of with a vacuum PC system is that the receiving vacuum has to be designed to withstand the vacuum (Mills, 2002). Vacuum pneumatic transfer is used over short and medium distances (around 2 to 80 m) (“Solutions for Pneumatic Conveying”) and has lower volumes of material conveyed compared to positive pressure systems. (Nowak, 2017; Purutyan, 2001). Vacuum systems are more restrained to dilute phase pneumatic conveying (Ortega-Rivas, 2017). In pneumatic conveying under vacuum, a positive displacement blower is placed after the collector and the collector is fitted with a cyclone filter to catch the particles and let the air out. An advantage of using vacuum for pneumatic conveying is its cleanliness – due to the vacuum, all the materials are sucked inward into the system, meaning cleanliness is maintained and dust leakages in the open atmosphere are avoided (Nowak, 2017; Ortega-Rivas, 2017). Therefore, vacuum systems are also commonly used in the pharmaceutical industry (Nowak, 2010). In addition to this, the air that is being conveyed through a vacuum system usually originates from an ambient area which mean that the effect of air temperature on the solids and conveying are miniscule. Contrarily, a positive pressure system could be blowing warmer air through the pipeline due to the adiabatic heat of compression, which could influence the solids being conveyed e.g. softening of the materials (Hilbert, 2019).

Due to the versatility of dilute phase PC and its economical investment cost (Pelletron, 2018) and the vacuum system capitalizing on cleanliness and low contamination and ease of material feeding (Hall, 2012), a vacuum, dilute phase, PC system will be used for this project.

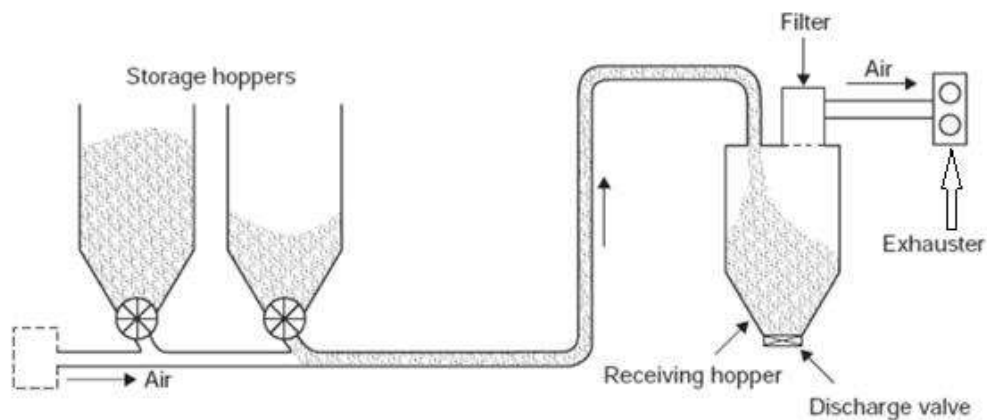


Fig. 2.1.3.1. A typical negative pressure PC system (adapted from Mills, 2002).

### 2.1.4. Saltation Velocity & Choking Velocity

In essence, the definition of saltation velocity and choking velocity is nearly the same. What differentiates them are the applications of each one and what it means for the PC system. The saltation velocity is applicable in horizontal pipes. The saltation velocity is the gas velocity at which the solid particles begin to "salt" or settle out of their suspended flow (dilute phase) in a horizontal pipe. As a

result, the solids no longer "fly" across the conveying pipes. At velocities slightly lower than the saltation velocity, the solids begin to move in a saltating flow where particles settle out and get re-entrained in the gas stream. Further below that velocity, the bottom layer of particles becomes thicker and dune flow is encountered (Rhodes, 1998; Ortega-Rivas, 2017).

The concept of choking velocity is just the same as the saltation velocity however it is used for vertical flow with the solids being conveyed upwards. If the gas velocity is gradually reduced while maintaining the same solids-air ratio, the system will reach a point where the gas velocity is not enough to maintain a dilute phase flow – the solids will start falling back on itself (into the gas stream) and will begin to flow sluggishly or bubbly. This point is known as the choking point. If the gas velocity is reduced even more, the sluggish flow will continue until the slip velocity is reached (slip velocity is the difference between the gas velocity and the particle velocity). Below this point, the slug flow will stop altogether and become a packed bed (Leung et al., 1971).

Because of the fact that the saltation velocity is higher than the choking velocity, applying the saltation velocity as the minimum velocity will prevent choking (Rhodes, 1998; "Choking Velocity in Pneumatic Transport"). The saltation velocity is higher than the choking velocity because it's more difficult to keep solids suspended in a horizontal line compared to a vertical line ("Reduce Velocity and Prevent Buildup"). In literature, there are many saltation velocity equations. Some are theoretical and some are empirical. It was made clear, however, that some of the correlations predicted widely differing velocities, even though the same set of conditions were applied (Ortega-Rivas, 2017). This leads to an important realization: one correlation cannot fit all PC applications. Rhodes (1998) elucidated that the correlation by Zenz, was frequently used. In addition to that, the Zenz correlation is completely empirical and makes use of a graph. The Zenz correlation has an average error margin of around 54%. The Zenz correlation (1964) (Ortega-Rivas, 2017) is shown in the appendix.

## 2.2. Equipment and Material

Table 2.2.1. List of Equipment used for PC Experiments

<b>Equipment</b>	<b>Apparatus Name/Series/Model</b>	<b>Function</b>	<b>Notes</b>
Laser Diffraction	Malvern; Mastersizer 3000	Measures the frequency and oversize (cumulative size) of the solids - particle size distribution	Particle size range: 0.01-3500 $\mu\text{m}$ for wet and dry dispersions (sysmex.nl)
Particle Imaging	Malvern; Morphology G3S	Analyzes the particle morphology – particle shape distribution	5-megapixel digital camera; can capture images of particles ranging from smaller than 0.5 $\mu\text{m}$ to larger than 3000 $\mu\text{m}$
Weight Balance	Toledo or Sartorius	Measures the mass (in grams) of an object down to the third/fourth decimal	Indicates the number of ten thousandths (4 zeros behind decimal point)
Flowmeter	Key Instruments; model MR-3A18-BVBN	Measures the flowrate of gas through the PC system	Flowrate range of 0 to 100 lpm
Flowmeter	Key Instruments model 2540A5A53PI	Measures the flowrate of gas through the PC system	Flowrate range of 100 to 700 lpm



Vacuum Pump	Eurovacuum; V025	EVDR-	Creates pressure difference in PC system for conveying	Flowrate ranging from 0 to 416 lpm
-------------	---------------------	-------	--	------------------------------------

Table 2.2.2. List of Materials used for PC Experiments

Material	Source/Brand/Batch	Function	Notes
Lignin Powder	Stora Enso	Benchmark material	Reference material $\geq 250$ micrometers
Cocoa powder	Blooker (Albert Heijn)	Benchmark material	21% fat content
Rubber granules	Granuflex	Benchmark material	0.8 – 2.3 mm in diameter
Copper pipes, copper bends, a variety of fittings, Teflon tape	Hornbach	Build the lab-scale PC setups	-
Small bottles	Delft Solutions	Solids Acts as the collector	Made of hard plastic, able to withstand vacuum.
Filter paper		Stop particles from entering flowmeter and pump	-
Ethanol	-	Cleaning	-
Acetone	-	Cleaning	-

## 2.3. Materials

### 2.3.1. Friable Materials

When solids undergo pneumatic conveying, especially in dilute phase, there is a chance that the solids will degrade i.e. shatter and break. The main cause of this is the particle velocity, where in dilute phase PC, must be kept high to maintain suspension flow. When particle breakdown readily occurs, the material is said to be friable. There are three tendencies of these breakdowns: the first is the shattering of the particle due to impact forces. The second is attrition, where fines and small pieces of the main particle can be worn off due to rubbing of the particles with other particles or with the wall or bends. The final tendency is angel hairs or streamers formation for nylons and polymers due to micro-melting when they slide against the pipeline wall or bend (Mills et al., 2004; Pelletron, 2018).

Semi-brittle failure is the main point of the friable material (lignin) for this project. Semi-brittle failure mode occurs when the plastic flow (occurs when impact stress exceeds the yield) of an object is limited. This causes cracks to form. Based on the crack morphology and extension, semi-brittle failure can present itself in two ways: fragmentation – occurs by the formation of median and radial cracks, and chipping – occurs by the formation of lateral cracks (Ghadiri, 2006). Lignin particles, based on past experiences/projects conducted by Delft Solids Solutions as well as the clients that provide Delft Solids Solutions with the lignin, are brittle, meaning that with a certain amount of stress, they don't deform. Adding increased amounts of stress will not change the strain on the material that much until a certain point. Since brittleness is not defined, this point is also not well defined. For brittle materials failure tends to occur before any noticeable elongation of the material (US Naval Academy). *Figure 2.3.1.1* shows the behavioral difference between brittle materials and ductile materials.

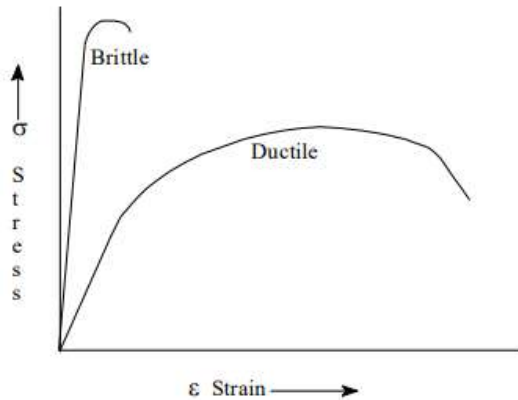


Fig. 2.3.1.1. Stress-strain relationship of brittle and ductile materials (US Naval Academy).

This semi-brittle failure can be further elucidated in the manner of how it would fail. It has been made clear that the lignin particles do not deform very much and tend to break when the stress exceeds a certain intensity. The types of breakage can be explained by van Laarhoven (2010) as shown by Fig. 2.3.1.2 below.



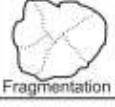

Magnitude	Direction	
	Normal	Tangential
Low force "Wear"	 Attrition	 Abrasion
High force "Fracture"	 Fragmentation	 Chipping

Fig. 2.3.1.2. Different ways a particle can break (van Laarhoven, 2010).

Fig. 2.3.1.2 can be simply explained by imagining what would happen to mildly spiky ball of chalk if it were thrown against a wall. If the chalk was thrown directly at the wall at low force, it would likely break edges off, making it more spherical. If the chalk was thrown really hard, the whole rock would break or shatter into pieces. Now, imagine holding the chalk rock, letting the other end of the rock touch the wall, and running alongside the wall, drawing a line on the wall in the process. If the running speed used is low, thus low force, then the outermost layer of the chalk rock would be rubbed off onto the wall, causing abrasion. If the running speed was increased (higher force), the part of the chalk rock rubbing the wall would chip off due to the strong tangential forces. A list of particle and environmental properties that affected particle strength was also provided by van Laarhoven (2010), as can be seen in the Table 2.3.1.1.

Table 2.3.1.1. Properties that affect the particle strength (van Laarhoven, 2010).

particle	environment
size	humidity
shape	temperature
history	velocity
porosity	direction of forces
mechanical properties	shear

### 2.3.2. Heat Sensitive Materials (Agglomeration)

Agglomeration is the process of random sticking between particles due to physical or chemical forces. This creates a larger aggregate which is porous and extended. Several techniques are used to create agglomerated products: 1) Pressure methods; 2) Tumble/growth and agitated methods; 3) thermal processes; 4) spray techniques. Agglomeration techniques can also be divided into “dry” and “wet” methods based on the type of binder used. The latter is usually referred to as granulation. In the process of agglomeration, the magnitude of particle binding depends on the size, structure, and moisture content of the particles (Kian-Pour et al., 2021).

There are four major mechanisms that allow particles to agglomerate and it is possible that more than one mechanism may apply for a given agglomeration process. These mechanisms are liquid bridges, solid bridges, intermolecular and intramolecular forces, and mechanical interlocking (Kian-Pour et al., 2021). Pneumatic conveying is done in dry conditions (low relative humidity) because if sufficient moisture is present, the materials could stick to the pipeline walls and over time, it could cause material buildup in the conveying line, pipeline blockage, and changes in the particle’s physical characteristics, especially if the particle can readily absorb water. Materials with high oil or high fat content can also cause severe buildup (Hilbert, 2019; Ortega-Rivas, 2017). For high fat cocoa powder, the most likely agglomeration mechanism that is present is solid bridges. What occurs is that due to inter-particle or particle-pipeline wall/bend impact forces or sliding (in dilute phase conveying), the contact points on the particles become heated. This causes partial melting and the molecules of one particle diffuse with the molecules of the adjacent particle. The high fat content also contributes to the formation of solid bridges by the melting and recrystallization of fat, known as melt agglomeration (Kian-Pour et al., 2021).

### 2.3.3. Highly Elastic Materials (Elongation)

When an object experiences force over a certain unit area, it experiences stress. Stress causes the object or material to deform – there is a displacement. This displacement is measurable and known as strain. Under low stress, an object can have linearly proportional strains, and this is valid for many materials. As an object experiences strain proportional to the stress, it is said to obey Hooke’s law. An object or material where Hooke’s law applies is said to be an *elastic body*, meaning that when the stress is removed, the object returns to its natural/original shape. In Fig. 2.3.3.1 below, a graph showing the relationship between stress and strain is presented. Even after the stress exceeds the proportionality limit, if the stress is gradually reduced, the object can still return to its original shape. This, however, is limited by the elastic limit, which is the point that once the stress exceeds, the material would not be able to return to its original shape. Another name for this elastic limit is the yield strength (US Naval Academy). It is after this point that plastic deformation is said to have occurred (“Elastic Properties of Materials”). Another thing that occurs past the elastic limit is strain hardening – the material is permanently strained to increase the yield strength (US Naval Academy). Therefore, a highly elastic material means that the material is able to deform to great limits or experience large stress and thus large strain, but once the stress is removed, it can return to its original shape. In other words, its elastic limit has an exceptionally high value.

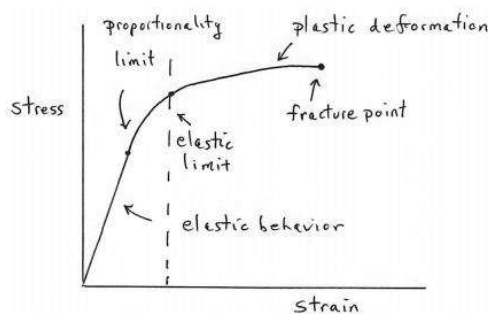


Fig. 2.3.3.1. Stress-strain relationship (“Elastic Properties of Materials”).



In industries that handle plastic materials, typically in pelletized form, particle melting could occur, especially when the conventional pipeline is used. The end-product of the melting of these plastics/polymers have many names such as angel hairs, streamers, raffia, or snake skins. They frequently cause blockages in the filters and diverters and need to be cleaned out, interrupting production. This is also a quality control issue since angel hairs are undesired in their polymer product. The mechanism of angel hair production is as follows: during pneumatic conveying, the polymeric granules will bump against the pipeline walls or bends. If the inner walls of the pipeline are smooth, the pellets will slide. When there is this contact, the particles decelerate due to friction, and friction is turned into heat. This heat is enough to deform the polymer pellets, stretching them out into angel hairs (Mills et al., 2004). This implies that the temperature of the contact points on the pellet increased to the glass transition temperature of the polymeric material, which converted the brittle behavior of the pellet to rubbery and plastic behavior, allowing it to elongate (Alderliesten, 2010). Fig. 2.3.3.2 displays the non-linear stress-strain relationship of polymers: a certain amount of stress can give a relatively extreme amount of strain.

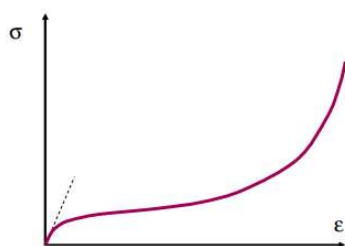


Fig.2.3.3.2. *Qualitative diagram of the non-linear stress-strain behavior of polymers (Alderliesten, 2010).*

There are many types of polymers and they have a wide variety of applications. Three main categories of polymers are: elastomers, plastics, and fibers. Rubbers (the product that will also be used for the project) is a type of elastomer, mainly characterized by its flexibility (high capability to return to its original shape, large strain to failures, non-linear stress-strain curves, and strain hardening (Alderliesten, 2010; Valentini & Lopez-Manchado, 2020). What gives rubber its staggering flexibility and also hardness is the vulcanization process, which prevents the polymer chains from moving independently. As a result, when stress is applied, rubber will deform, but as soon as the stress is taken away, rubber can come back to its original shape (Valentini & Lopez-Manchado, 2020). The rubber used in this project is natural rubber (NR). It is used in tires, footwear, and coatings, to name a few applications. It has an operation temperature between -55 to 70°C and its glass transition temperature is -62°C (Hanhi et al., 2007; Schawe, 2007).

## 2.4. Analytical Methods

### 2.4.1. Laser Diffraction Spectrometry

Laser diffraction spectrometry, laser diffraction, or laser light scattering is a widely employed technique that is used to analyze particle size and particle size distribution. Laser diffraction will give a volume weighted distribution (Eshel et al., 2004; Barbosa-Canovas et al., 2005; Malvern Instruments Limited, 2015). It falls under one of the four main methods to determine size distribution: stream scanning. In stream scanning, particles are suspended and exposed to a restriction or various light sources. The response that is obtained is a function of the concentration and number of particles present. The other three are sieving, microscope counting techniques, and sedimentation (Ortega-Rivas, 2017). The main principle of laser diffraction is the scattering of a light beam due to the presence of particles (in an air or liquid stream). The laser diffraction particle size analyzer measures the angle and intensity of the scattered light after hitting the particles ("A Basic Guide to Particle Characterization"). In this project, the instrument called the Mastersizer 3000 by Malvern is used for laser diffraction.

This scattered light consists of reflected and refracted waves. Reflected or diffracted waves take place due to edge phenomena – diffraction is dependent only on the geometric cross-section of the particle. On the other hand, light can also be absorbed or refracted. The absorption takes place because once the light waves strike the particle, there is a conversion of energy. This attenuates the light intensity (Hackley et al., 2004). The particle size is inversely proportional to the angle width and the wider the angle the weaker the light intensity. So, a small particle will scatter light at a wide angle and the light intensity will be low, while a large particle will scatter light at a low angle and the light intensity will be high (Eshel et al., 2004). This difference will also complicate detecting the presence of a small concentration of fine particles in a matrix of predominantly larger particles. This can be seen in *Fig. 2.4.1.1*. The next 2 figures, *Fig. 2.4.1.2* and *Fig. 2.4.1.3*, show the light scattering mechanism and laser diffraction system respectively.

The primary material property that affects scattering (besides the size and shape of the particle) is the refractive index  $m = n - ik$ .  $n$  and  $k$ , also known as optical constants, are the real and imaginary absorptive components, respectively. Scattering itself, arises from the difference in refractive index (real component) between the particle and the medium (Hackley et al., 2004). The size range covered by these instruments is approximately 2 to 500  $\mu\text{m}$  (Ortega-Rivas, 2017). Barbosa-Canovas et al. (2005) reported a much larger range for laser diffraction instruments: 0.1 to 3000  $\mu\text{m}$  while Malvern Panalytical ("Laser Diffraction Particle Size Analysis") stated a measurable particle size range from 0.01 to 3500  $\mu\text{m}$ .

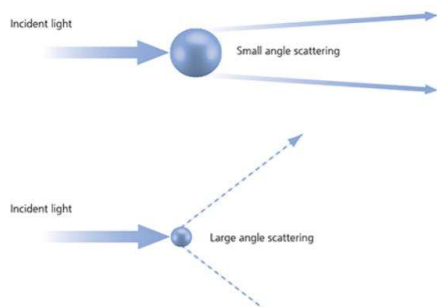


*Fig. 2.4.1.1. Scattering angles of large and small particles (Malvern Instruments Limited, 2015).*

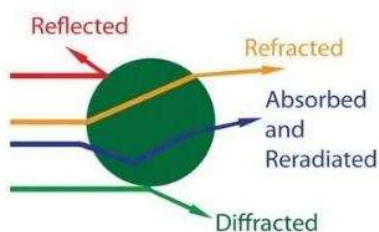


*Fig. 2.4.1.2. The scattering of light when it hits a particle ("A Basic Guide to Particle Characterization").*

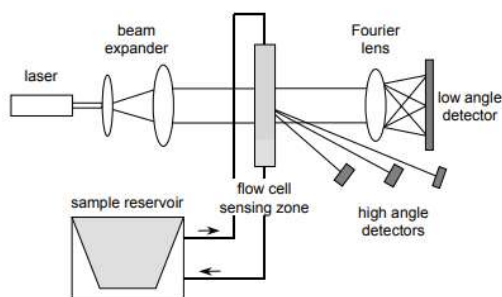


*Fig. 2.4.1.3. Diagram of the working principle of a laser diffraction system (Hackley et al., 2004).*

### 2.4.2. Particle Imaging Microscopy

#### Size

Microscopy is one of the oldest techniques used to determine the size and size distribution of fine particles. The reason why microscopy is used in this project is to analyze the particle shape. In this project, the instrument by Malvern named Morphologi G3 is employed for particle imaging microscopy. The Morphologi G3 is able to measure the size and shape of particles and it can do so with particle sizes ranging from 0.5 to 3000  $\mu\text{m}$  (Malvern Instruments Limited, 2008; Ortega-Rivas, 2017).

Particles are normally difficult to describe with a single number due to their irregular shape. However, these irregular particles can be described using a number of particle sizes (Ortega-Rivas, 2017; Malvern Instruments Limited, 2008). The circle equivalent diameter is what the Morphologi G3 uses to characterize a particle size. It does so by capturing a 2D image of the particle and converting it to a circle with an area equivalent to that of the 2D image (Morphologi G3 manual). An illustration of how it does so is shown below in *Fig. 2.4.2.1*.

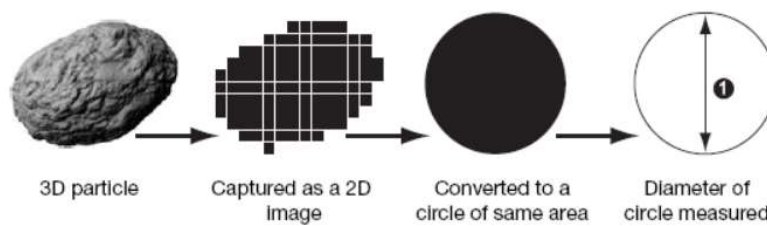


*Fig. 2.4.2.1. Equivalent circle diameter determination method by the Morphologi G3 (Malvern Instruments Limited, 2008).*

#### Shape

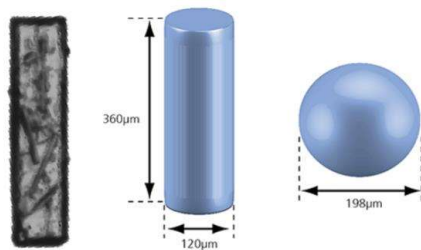


*Fig. 2.4.2.2. Image of a needle-like particle and its cylindrical dimensions and spherical diameter based on the volume (Malvern Instruments Limited, 2015).*

The next important factor that needs to be taken into account when characterizing a particle is the shape. A disadvantage of using only particle size for characterization is that minor differences in the particles are overlooked during translation to circle or sphere equivalent (*Fig. 2.4.2.2*, right image) diameters and very differently shaped samples could be identically characterized only because they have similar 2D projections (Malvern Instruments Limited, 2008; Malvern Instruments Limited, 2015).

There are three commonly used shape factors: circularity, convexity, elongation. They are described below (Malvern Instruments Limited, 2008).

#### Circularity

A way to measure the shape by quantifying how close it is to a circle. It could also be thought as the deviation from a perfect circle. Circularity is defined as the ratio between the perimeter of a circle with an area equal to that of the particle and the perimeter of the actual particle image. Circularity has a value

range with perfect circles being 1 and more irregular or spiky particle being closer to 0. Using circularity only, however, is not sufficient to discriminate all the different applications and combinations of shapes, as is demonstrated by *Figure 2.4.2.3* below – the top right and bottom left particles have the same circularity. For that reason, 2 more descriptors are used – convexity and elongation.

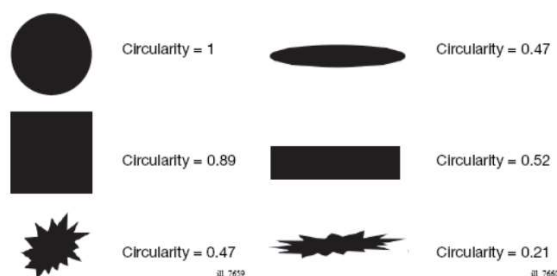


*Fig. 2.4.2.3. Different shapes and their corresponding circularity values (Malvern Instruments Limited, 2008).*

### Convexity

Convexity is the measurement of how rough a particle is and its value is obtained by dividing the **convex hull perimeter** by the actual particle perimeter. The convex hull perimeter can be easily illustrated as a rubber band that goes around the particle indicated by the dotted line, as seen in *Figure 2.4.2.4*.

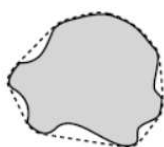


*Fig. 2.4.2.4. A random particle shape and its convex hull perimeter shown by the dotted lines (Malvern Instruments Limited, 2008).*

Smoother surfaces are closer to 1 and rougher or spikier surfaces are closer to 0. *Fig. 2.4.2.5* shows a few convexity examples and how a smooth circle and a smooth needle can both have a convexity of 1.

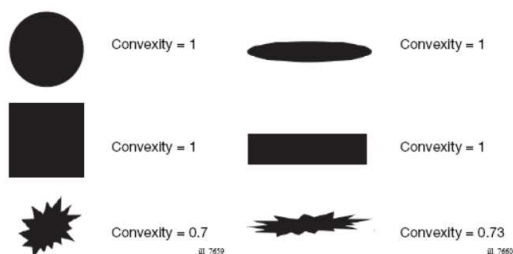


*Fig. 2.4.2.5. Convexity of different shapes and different spikiness (Malvern Instruments Limited, 2008).*

### Elongation

The definition of elongation is 1 minus aspect ratio – aspect ratio is width divided by length. Elongation has a range from 0 to 1. A particle is symmetrical in all axes such as a square or a sphere has an elongation value of 0. If that particle has a larger aspect ratio, then the elongation will be closer to 1. It is worth mentioning that elongation is not influenced by surface roughness as can be seen by the top right and bottom right shapes in *Fig. 2.4.2.6*.

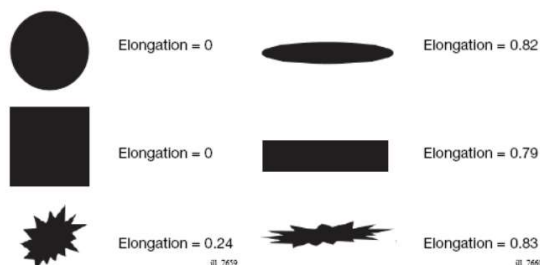


Fig. 2.4.2.6. Different shapes and their elongation values (Malvern Instruments Limited, 2008).

### 2.4.3. Sieving

Sieving is one of the techniques used to determine particle size and particle size distribution. It is a simple, reproducible, and inexpensive method for particle size analysis and applies the principle of geometry similarity. It is also the only known particle size analysis technique to provide a particle size distribution based on particle mass. All types of sieving cover a range between 5  $\mu\text{m}$  and 4 mm. The sieving machine shown in Fig. 2.4.3.1 is unable to sieve down to 5  $\mu\text{m}$ . The lower limit can be achieved using micro-mesh sieves while the higher limit can be achieved by using punch-plate sieves. The lower limit is limited to the determined mesh size for two reasons: the production of a sieve cloth that is fine enough for smaller particles is impossible and the gravity force of fine powders isn't, strong enough to overcome the adherence of particles to one another or to the sieve cloth (Barbosa-Canovas, 2005). Eshel et al. (2004) reported that sieving is appropriate for a particle size range from 50 to 2000  $\mu\text{m}$ .

A standard sieve series normally consists of a set of sieves with a wide range of apertures (squares in the mesh through which the particles pass through) from micrometers to centimeters. The size of the sieve is determined by the aperture size and the aperture size is determined by the size of the mesh and wire. When the sieves are placed in order in a series, the ratio between the aperture size in one sieve to the aperture in the next sieve is constant. Fig. 2.4.3.1 shows an example of one sieve and a stack of sieves. Sieving analysis is conducted by stacking the sieves in ascending order according to the aperture size (larger aperture is placed higher on the stack), placing the material to be sieved on the top sieve, and vibrating the sieves for a fixed amount of time, either by hand or with a machine. Liquid flow, air-jet, or vibrating air column can be used to assist the sieving process (Barbosa-Canovas, 2005).



Fig. 2.4.3.1. A sieve (left) and a stack of sieves (right) ("Different Sieving Methods for Varying Applications").

## 3. Methodology

The goal of this project was to identify and quantify the effects of dilute phase pneumatic conveying on friable materials, heat sensitive materials, and elastic materials. According to this goal, several experiments were designed with a handful of variables such as the conveyed materials, pipeline diameter, pipeline orientation (horizontal or vertical), and conveying velocity. After running the pneumatic conveying system, the solids were further analyzed to quantify the changes that were experienced by the conveyed materials. The design of these experiments as well as the method of analysis are discussed in this chapter.

### 3.1. Pneumatic Conveying System Design

The first setup used an outer pipe diameter of 12 mm and oriented horizontally. This was made the "small" diameter pipeline. The reason for this was to follow up on the previous research. In the second setup, the diameter was nearly doubled to an outer diameter of 22 mm. This became the "large" diameter pipeline. The purpose of the larger diameter was to simulate industrial conditions (which also used large-diameter pipes, even larger than 22 mm). The orientation was also horizontal. The third setup used an

outer pipe diameter of 22 mm as well. However, the orientation was made vertical – the solids were to be conveyed upwards. This third setup was created in order to compare the effects on pneumatic conveying between a horizontal setup and a vertical setup.

For each setup, two bend numbers were determined: three bends and nine bends – they were "low" number of bends and "high" number of bends, respectively. This was done to compare how an increase in bend number would influence the particles. *Table 3.1.1* shows the setups used for each material.

*Table 3.1.1. Variation of setups used for each material.*

	12mm horizontal (H)	22mm horizontal (H)	22mm vertical (V)
3 bends (3B)	12mm H 3B	22mm H 3B	22mm V 3B
9 bends (9B)	12mm H 9B	22mm H 9B	22mm V 9B

### 3.2. Determination of the Saltation Velocity

The Zenz correlation, as described in chapter 2, was used to determine the saltation velocities. The three materials had saltation velocities that ranged from 2-5 m/s. The selected conveying velocities therefore, were higher than the saltation velocities. Several tests were executed in order to find which velocity could be considered low but still allow a sufficient amount of the material to be successfully conveyed. The low velocities that were selected can be read in *Table 3.2.1* below. As for the high velocities, only one was used for all the materials. This one velocity was used because it was the highest that the pump could provide, but also allow for a fair comparison between different pipe-diameter setups for a single solid.

*Table 3.2.1. A list of low and high velocities used for the materials in the experiments*

Solids	Low Velocity (m/s)	High Velocity (m/s)
Lignin particles	7.44	18
Cocoa Powder	9	18
Rubber Particles	9	18

### 3.3. Extra Hardware

In order to make pneumatic conveying possible, a pump was purchased. A vacuum pump from Eurovacuum model type EVDR-V025 was ordered. It had a maximum volumetric flow rate of 25 m<sup>3</sup>/h or 416.67 liters per minute. The maximum vacuum it could create was 150 mbar. In order to be able to measure the flowrate exactly, two flowmeters were ordered from RS Components. The first had a flow range from 0 to 100 liters per minute while the second had a flow range of 100 to 700 liters per minute. The collectors for the PC system was made by hand. The collector was made with a small cylindrical container, filter paper, and hole making tools. The collector was designed to have an inlet for the particles and an outlet for the air. The outlet was covered with a filter paper. *Fig. 3.3.1* & *Fig. 3.3.2* show the design of the collector. This was used for the 12 mm horizontal setup. For the 22 mm horizontal and vertical setups, a large collector was made, although the concept was similar to the one in *Fig. 3.3.1*.





Fig. 3.3.1. The parts of the collector.

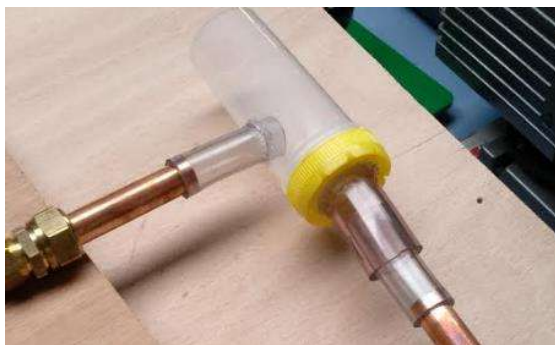


Fig. 3.3.2. The collector when connected to the piping system. Solids inlet is on the left; gas outlet is on the right.

### 3.4. Experimental Procedures

#### 3.4.1. Lignin

The goal of pneumatically conveying lignin particles (friable material) was to quantify its breakage rate when pneumatically conveyed. Before pneumatic conveying, the lignin particles were first sieved through a 250  $\mu\text{m}$  sieve. The sieving process was done to remove the fines. All particles larger than 250  $\mu\text{m}$  in diameter were kept and used for the lignin experiments. Approximately five grams of lignin particles were weighed and pneumatically conveyed. PC was done within 100 seconds, giving an average dosing rate of 0.1 gr/sec. The particles were taken out of the collector and weighed. This was post-PC lignin. The post-PC lignin weight was compared with pre-PC lignin weight to determine product loss in the conveying pipeline. The filter paper was also weighed to measure the fines stuck on the filter paper. The post-PC lignin was sieved again for 3 minutes and the particles that remained above the sieve were weighed, giving post-sieve lignin. This was compared to the weight of the lignin in the beginning (before PC) and breakage was calculated. The fines of the sieving process were re-added with the post-sieve lignin and the change in particle size distribution was quantified with laser diffraction. Benchmark for 0 bar was created. 0 bar was used, feed rate of 20%. Lignin particulate characteristics: refractive index is 1.6; absorption index is 0.1; and density is 1.3  $\text{g/cm}^3$ .

#### 3.4.2. Cocoa powder

The goal of pneumatically conveying cocoa powder (cohesive material) was to see whether agglomeration (which could potentially cause pipe blockage) took place when pneumatically conveyed. Approximately 5 grams of cocoa powder was weighed and pneumatically conveyed in 60 seconds, which gave an average dosing rate of 0.1 gr/sec. The cocoa powder was removed from the collector and weighed again. This was post-PC cocoa powder. The post-PC cocoa weight was compared with pre-PC cocoa weight to determine product loss in the conveying pipeline. Then the post-PC cocoa powder and cocoa powder that remained in the pipe were analyzed using laser diffraction to check for agglomeration or any changes in the particle size distribution. The laser diffraction setting used for cocoa powder was a refractive index of 1.59, absorption index was 0.1, and density was 0.36  $\text{g/cm}^3$ .

#### 3.4.3. Rubber particles

The goal of pneumatically conveying rubber particles (highly elastic material) was to identify and quantify deformation (if any) when pneumatically conveyed. Approximately 5 grams of rubber particles was weighed and pneumatically conveyed in 50 seconds, which gave an average dosing rate of 0.1 gr/sec. The rubber particles were recollected from the collector and analyzed using microscopy to identify and quantify the deformation. The lens used for the microscope had a magnification of 2.5 times.

#### 3.4.4. Experiments executed

With the materials, PC design, and conveying velocities determined, the experimental design was complete. Tables 3.4.4.1, 3.4.4.2, and 3.4.4.3 below provides a matrix of all the conditions/variables used for each experiment for lignin, cocoa powder, and rubber particles, respectively.

*Table 3.4.4.1. Conditions used for PC experiments of lignin particles.*

	12 mm Horizontal (12H)	22 mm Horizontal (22H)	22 mm Vertical (22V)
3B; 7.44 m/s (Ulow)	12H 3B Ulow	22H 3B Ulow	22V 3B Ulow
3B; 19 m/s (Umax)	12H 3B Umax	22H 3B Umax	22V 3B Umax
9B; 7.44 m/s (Ulow)	12H 9B Ulow	22H 9B Ulow	22V 9B Ulow
9B; 19 m/s (Umax)	12H 9B Umax	22H 9B Umax	22V 9B Umax

- 1 Ulow = Low velocity
- 2 Umax = Maximum or highest velocity
- 3 B = Bends

*Table 3.4.4.2. Conditions used for PC experiments of cocoa powder.*

	12 mm Horizontal (12H)	22 mm Horizontal (22H)	22 mm Vertical (22V)
3B; 9 m/s (Ulow)	12H 3B Ulow	22H 3B Ulow	22V 3B Ulow
3B; 18 m/s (Umax)	12H 3B Umax	22H 3B Umax	22V 3B Umax
9B; 9 m/s (Ulow)	12H 9B Ulow	22H 9B Ulow	22V 9B Ulow
9B; 18 m/s (Umax)	12H 9B Umax	22H 9B Umax	22V 9B Umax

*Table 3.4.4.3. Conditions used for PC experiments of rubber particles.*

	12 mm Horizontal (12H)	22 mm Horizontal (22H)	22 mm Vertical (22V)
3B; 9 m/s (Ulow)	12H 3B Ulow	22H 3B Ulow	22V 3B Ulow
3B; 18 m/s (Umax)	12H 3B Umax	22H 3B Umax	22V 3B Umax
9B; 9 m/s (Ulow)	12H 9B Ulow	22H 9B Ulow	22V 9B Ulow
9B; 18 m/s (Umax)	12H 9B Umax	22H 9B Umax	22V 9B Umax

## 4. Results and Discussion

To quantify the breakage of lignin, agglomeration of cocoa powder, and deformation of rubber particles, during pneumatic conveying, several parameters for the experiments were established which were velocity, pipe diameter, pipeline system orientation, and the number of bends. The results gathered from the consequent experiments are analyzed and discussed in this chapter.

### 4.1. Lignin

Three sets of experiments were executed for the lignin particles. The first set was done in the 12 mm (diameter) horizontal setup. In this set, two different number of bends (three bends and nine bends) were varied with 2 different velocities (7.44 m/s and 19 m/s). These were done to find out what the effects of **bend number** and **gas velocity** were. Thus, there were four experiments: (i) three bends, 7.44 m/s; (ii) three bends, 19 m/s; (iii) nine bends, 7.44 m/s; and (iv) nine bends, 19 m/s. These were duplicated resulting in a total of eight experiments for the 12 mm horizontal setup.

The second set was done in the 22 mm horizontal setup and the third was in the 22 mm vertical setup. Both these setups used three and nine bends as well as velocities of 7.44 m/s and 19 m/s just like the 12 mm horizontal setup. The 22 mm horizontal setup was created in order to find out what would happen



if the **pipe diameter** of the conveying pipeline was increased. The 22 mm vertical setup was created in order to find out what would happen if the **orientation** of the conveying pipeline was changed.

#### 4.1.1. 12mm Horizontal breakage percentage

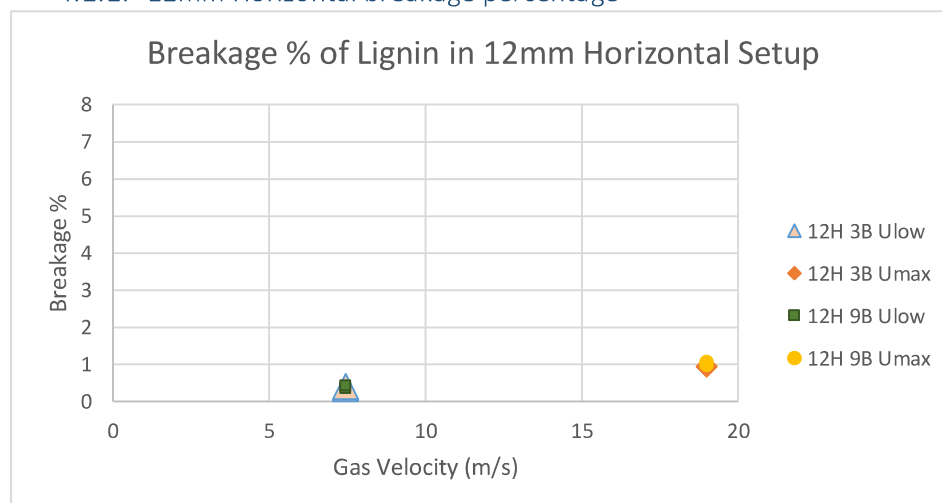


Fig. 4.1.1.1. Breakage values of lignin when conveyed through 12 mm horizontal setup.

Table 4.1.1.1. Breakage percentages of lignin in the 12 mm horizontal setup.

Exp. name	No.	Bends	Velocity (m/s)	Breakage (%)
12H 3B Ulow (Pink triangle)	1	3	7.44	0.3707
	2	3	7.44	0.4086
12H 3B Umax (orange diamond)	1	3	19	0.9627
	2	3	19	0.9452
12H 9B Ulow (green square)	1	9	7.44	0.3764
	2	9	7.44	0.4388
12H 9B Umax (yellow circle)	1	9	19	1.0659
	2	9	19	0.9957

Fig. 4.1.1.1 shows the breakage percentage of lignin in the experiments of the 12 mm horizontal setup. An occurrence that can be observed from the breakage percentage graph of the 12 mm horizontal setup is that at high velocity (19 m/s), whether it's three bends or nine bends (orange diamond and yellow circle, respectively), the breakage percentage is roughly two times higher than at low velocity (7.44 m/s). Increasing the number of bends also increases the breakage percentage, although the effects of increasing the bend number is less than increasing the velocity. Take for example the three bends and nine bends experiments at Umax (19 m/s) (orange diamond and yellow circle respectively) – the increase is only about 0.1% (0.95% to 1.05%). The values can be read from Table 4.1.1.1. This can be explained through the equation for kinetic energy:

$$E_k = \frac{1}{2} m (0.7 * V_{air})^2 * k \dots \dots \dots (\text{Eq. 4.1.1})$$

$E_k$  is the kinetic energy in joules or kilojoules.  $M$  is the mass of the particle in kilograms.  $V_{air}$  is the gas velocity in m/s. In this equation, the velocity of the particle is needed. According to van Laarhoven (2010), the particle velocity is usually 0.7 times the gas velocity, so this value will be used.  $K$  is a coefficient for the number of bends – the assumption is that each bend equals to one collision.

It can be seen from this equation that the value of the particle velocity is squared, while the number of bends is only proportional to the kinetic energy. This allows the particle velocity to have a greater influence on the kinetic energy. This is proven by the results of the breakage percentage in this 12 mm horizontal setup.

Another thing that can be observed is the greater variability in the breakage percentage when nine bends is used instead of three bends, no matter whether it's low velocity or high velocity. The bends used in the experiments are long radius bends, characterized by the ratio of the radius of curvature ( $R_B$ ) to the diameter ( $D$ ) of the pipe ranging from 8 to 14 (Dhodapkar et al., 2009).

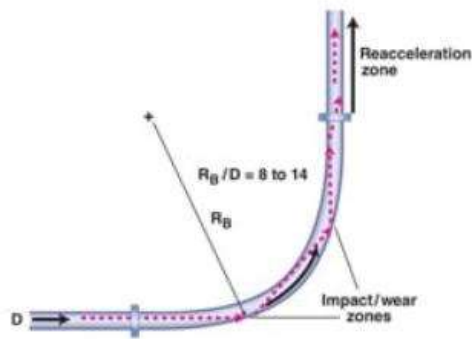


Fig. 4.1.1.2. Number of possible particle-wall impacts in a long-radius bend (Dhodapkar et al., 2009).

As can be seen from Fig. 4.1.1.2, there are a maximum of 4 impact zones or spots in the area of the bend and slightly after the curvature of the bend. If it is assumed that the best case scenario is one where particle-wall impact occurs once per bend and in the worst case scenario there are 4 occurrences of impact, then the maximum variation or difference between the least number of impacts (three bends times 1 impact per bend equals 3 total impacts) and the most number of impacts (three bends times 4 impacts per bend equals 12 total impacts) for a three-bend setup is nine impacts. For a nine-bend setup, that difference goes up to 27 impacts. Furthermore, the minimum number of impacts also rises from three to nine impacts when moving from three to nine bends, respectively. This can also explain why the minimum breakage value of lignin when conveyed with nine bends is higher than with three bends. This is valid for the low velocity and high velocity experiments.

#### 4.1.2. 22mm Horizontal breakage percentage

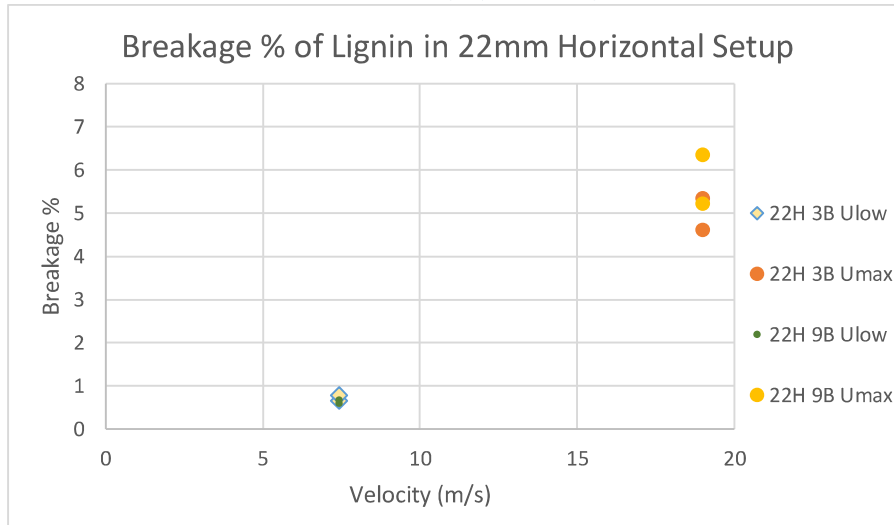


Fig. 4.1.2.1. Breakage values of lignin when conveyed through 22 mm horizontal setup.

Table 4.1.2.1. Breakage percentages of lignin in the 22 mm horizontal setup.

Exp name	No.	Bends	Velocity (m/s)	Breakage (%)
22H 3B Ulow (white diamond)	1	3	7.44	0.671
	2	3	7.44	0.7929
22H 3B Umax (orange circle)	1	3	19	4.6284
	2	3	19	5.3531
22H 9B Ulow (green circle)	1	9	7.44	0.6895
	2	9	7.44	0.5938
22H 9B Umax (yellow circle)	1	9	19	6.366
	2	9	19	5.2251

The most obvious difference that can be seen among the breakage percentages between the low velocity and high velocity experiments in Fig. 4.1.2.1 is that the breakage percentages of the high velocity experiments (orange and yellow circles) are around six to ten times greater than the breakage of the low velocity experiments (white diamonds and green circles). The numerical values can be read in Table 4.1.2.1. The high velocity (19 m/s) experiments (yellow and orange circles) also give a wider difference between breakage values compared to the low velocity experiments (7.44 m/s) (white diamonds and green circles). The latter also shows that at low velocity, no matter whether three or nine bends are used, the breakage values tend to remain concentrated around 0.6 and 0.7%.

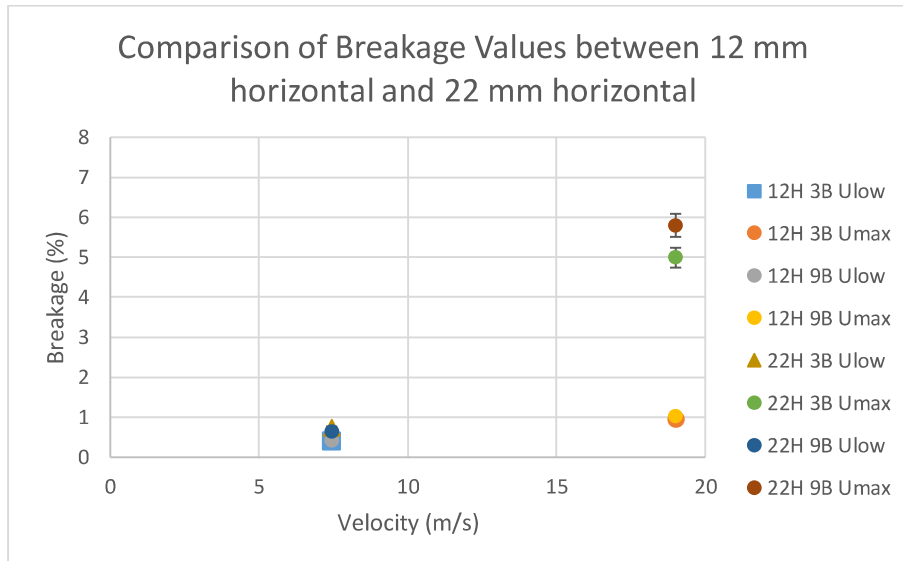


Fig. 4.1.2.2. Averaged breakage percentages from experiments in the 12 mm horizontal and 22 mm horizontal setups.

When comparing the breakage percentage results of the 22 mm setup to the 12 mm setup as seen in Fig. 4.1.2.2, it is very clear that all experiments (three bends and nine bends) conducted at low velocity are extremely repeatable and have an average breakage percentage of around 0.6%, which is very similar to the 12 mm horizontal setup. At high velocity, that value shoots up to an average of 5.39 % – an increase of almost 5%, compared to the 0.6% increase of the 12 mm horizontal setup. Firstly, the breakage percentage of lignin at low velocity for three bends and nine bends in the 12 mm and 22 mm horizontal setups can be similar due to the fact that the low velocities are saltation velocities, which are the minimum gas velocities that still allow a particular solid to be pneumatically conveyed. By using low velocities, the impact force no matter the diameter of the pipe, is the smallest possible. Thus, in the 3-bend experiments, the total kinetic energy or impact force on the pneumatically conveyed solids in the 12 mm horizontal setup is equivalent (or similar) to the 22 mm horizontal setup. The same can be said for the 9-bend experiments for both setups, although, the 9-bend experiments show slightly higher breakage percentages than the 3-bend experiments as well as higher breakage variation/difference compared to the 3-bend experiments.

Moving on to the high velocity part of the experiments, a broad range of values can be seen. Once again, the nine bends shows higher breakage variation than the three bends. In general, the breakage values of the high velocity experiments are about 5-6 % higher than the breakage values of the low velocity experiments in the 22 mm horizontal setup. When comparing these results (high velocity experiments, 22 mm horizontal pipe) to the high velocity experiments of the 12 mm horizontal setup as shown in Fig. 4.1.2.2, the breakage values are five to six times higher (depending on the bend number). Considering the fact that no other parameter changes except the pipe diameter (from 12 mm to 22 mm), then the explanation must have something to do with the flow of air in the pipes, which has an effect on the motion of the particles and their consequent collisions with the pipeline wall. This motion of air is also known as fluid flow, which could also include liquids. Fluid flows can be divided into laminar and turbulent flows. These 2 conditions can be determined by the Reynolds number (Re).

$$Re = \frac{\rho V d}{\mu} = \frac{V d}{\nu} \dots\dots\dots (Eq. 4.1.2)$$

$\mu$  is the dynamic viscosity and  $\nu$  is the kinematic viscosity ("Transition and Turbulence")

The Reynolds number is a dimensionless number. If the Reynolds number is smaller than 2300, then the flow was laminar. Above 2300 and the flow would become turbulent without exception. The equation suggests that laminar flow occurs for low speeds, small diameters, low densities and high viscosities while turbulent flow occurs for the opposite: high speeds, large diameters, high densities, and low viscosities. Therefore, the flow of air in the 22 mm pipe is more turbulent and prohibited the lignin particles from flowing in a steady stream, but instead flow in a disorderly fashion, where there are greater chances for particle-wall impact. This resulted in higher breakage percentages in the 3 and 9-bend, high-velocity experiments than in the same experiments conducted in the 12 mm pipe. It also caused a greater difference in the breakage yield at high velocity than in the 12 mm pipe.

#### 4.1.3. 22mm Vertical breakage percentage

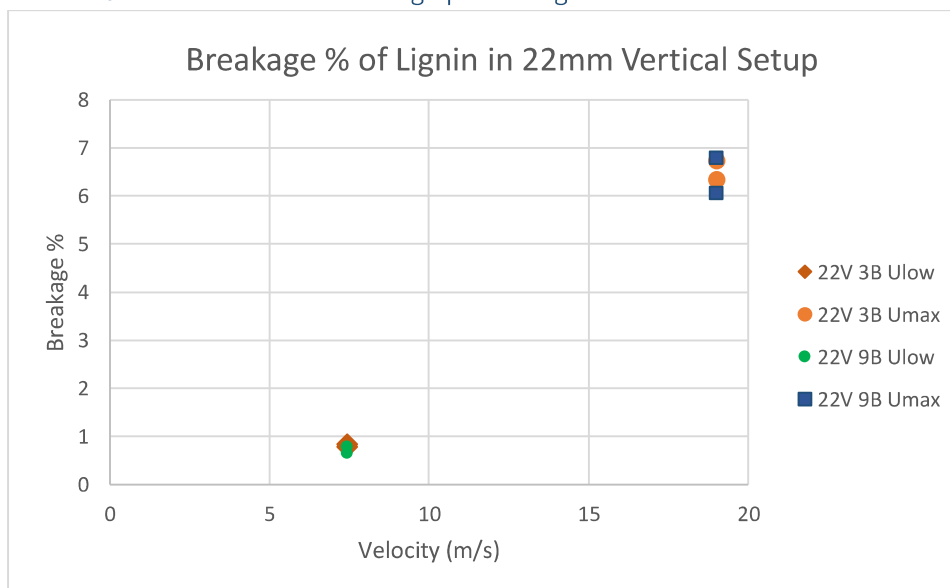


Fig. 4.1.3.1. Breakage values of lignin when conveyed through 22 mm vertical setup.

Table 4.1.3.1. Breakage percentages of lignin in the 22 mm vertical setup.

Exp name	No.	Bends	Velocity (m/s)	Breakage (%)
22V 3B Ulow (Brown triangle)	1	3	7.44	0.8356
	2	3	7.44	0.7801
22V 3B Umax (orange circle)	1	3	19	6.7373
	2	3	19	6.3435
22V 9B Ulow (green circle)	1	9	7.44	0.7778
	2	9	7.44	0.6522
22V 9B Umax (blue square)	1	9	19	6.0627
	2	9	19	6.7915

In the 22 mm vertical setup, a few things are directly noticeable. The first is that all experiments at low velocity exhibit similar breakage values. However, these 4 values are overall slightly higher than the 4 breakage values from the low velocity experiments of the 22 mm **horizontal** setup.

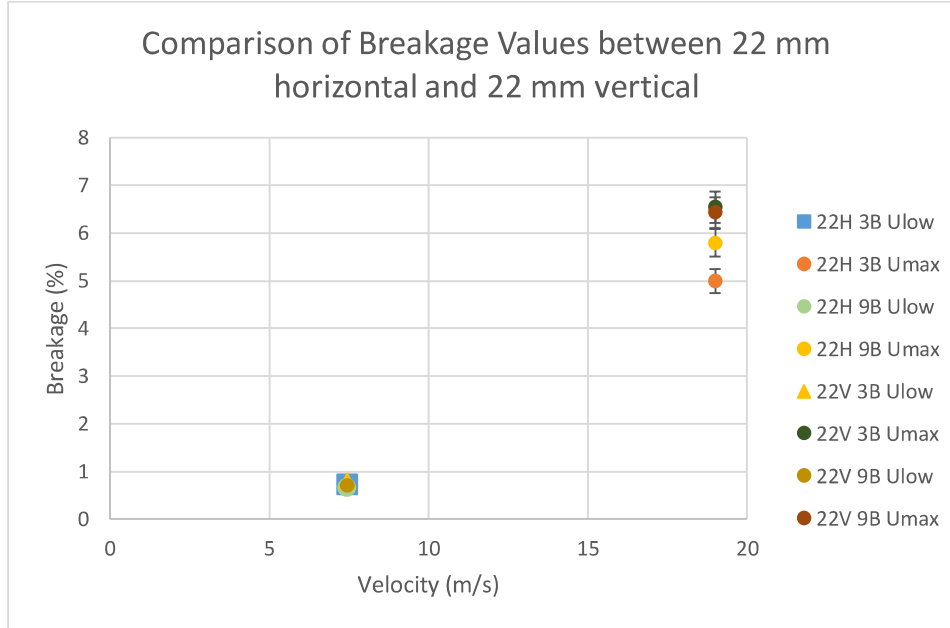


Fig. 4.1.3.2. Averaged breakage percentages from experiments in the 22 mm horizontal and 22 mm vertical setups.

When shifting to the higher velocity experiments, the 22 mm **vertical** setup generated higher breakage rates (all above 6 %) compared to the 22 mm **horizontal** setup (5-5.7 %). This is shown in Fig. 4.1.3.2. Once again there is a higher variation of breakage values from the nine-bend experiments instead of the three-bend experiments however when compared to the same experiments in the 22 mm horizontal setup, the breakage variation in this setup is not as pronounced. Moreover, the lowest breakage value at high velocity is achieved at nine bends instead of three bends, while the maximum breakage at high velocity for the nine bends overlaps almost perfectly with the three bends. In other words, the worst case breakage scenario of the nine bends and three bends are nearly identical and in the best case scenario (least breakage), the nine bends offers less breakage than three bends.

The higher breakage rates can be explained with the setup itself, since the only difference between the 22 mm horizontal setup and 22 mm vertical setup, as the name suggests, is the orientation of the setup. The 22 mm vertical setup is not purely vertical. It is actually a combination of horizontal sections and vertical sections. From the Fig. 4.1.3.3, that would be -X west to the intersection, to +Y up to +W. The way the particles travel and interact with the pipeline wall is therefore slightly different than how it would occur if all the pipes were on a horizontal plane, or if, based on the figure below, the particles traveled from -X west to +X1 or +X2 via +Z south or -Z north, respectively.

Looking again at Fig. 4.1.3.3, the first point of interest is the intersection between -X west, +X east, +Z south and -Z north. When particles approach the intersection and hit the bend there, the initial particle impact will be similar no matter whether the bend is directed to +Z south, -Z north, or +Y up. When the particles reach the +Z south to +X1 bend or -Z north to +X2 bend, the impact pattern from the intersection impact is replicated. On the other hand, when the particles reach the +Y up to +W bend, an interesting impact pattern is observed. Lignin is a low density material. As explained by Tripathi et al. (2018), when non-dense solids are conveyed in a vertical pipe, the particles tend to get scattered towards the pipe wall. The particles closer to the outer bend wall will experience more sliding forces against the pipe wall while the particles further away from the outer bend wall will experience more collision-like forces. This can be seen in the bend in Fig. 4.1.3.4.

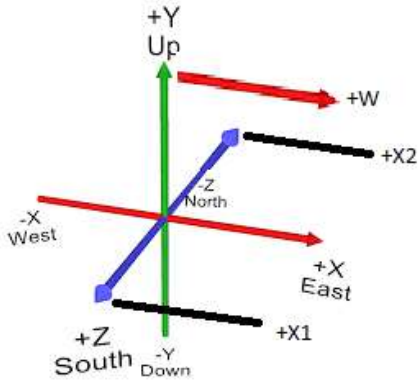


Fig. 4.1.3.3. Illustration of “horizontal” vs. “vertical” setups.

The following impact pattern becomes crucial here. As seen in Fig. 4.1.3.4, the particles, after making the first impact with the bend, travel further down the horizontal pipe and make a second impact on the bottom of the pipe. This would be an impact in the +Y up – +W “pipe”. At impact with the bend, there is a deceleration of the gas, which consequently decelerates the particles. What occurs is that the particles (still containing kinetic energy) are deflected from the “outer curve” of the bend towards the horizontal pipe – it is the direction of the particles’ “bounce”. The direction of the deflection makes the particles travel downwards, like in Fig. 4.1.3.4. This force of the particles when making the second impact in the horizontal pipe is increased by the presence gravity that is simultaneously pulling the particles downwards. So the total force from the second impact at a specific spot in the horizontal pipe originates from the deflected particles that contain kinetic energy plus the gravitational force. It could be imagined as how would a ball behave if it was thrown against a ceiling vs. if it was thrown against a wall.



Fig. 4.1.3.4. Movement of particles from vertical to horizontal pipe during pneumatic conveying.

From the breakage percentages obtained, it can be seen that in the 12 mm horizontal setup, whether the gas velocity is 7.44 or 19 m/s or the bend number is three or nine, the breakage percentage ranges from 0.3-1 %. In the 22 mm horizontal setup, a low gas velocity creates minimum breakage of around 0.5-0.7 %, similar to the 12 mm horizontal setup. At high gas velocity, the breakage percentage increases by at least 7 times – average breakage at high velocity with three and nine bends is 5.3 %. A greater difference in duplicates is seen as well when nine bends are used than in three bends. Maximum breakage is 6.4 %. Finally, in the 22 mm vertical setup, the low velocity experiments produced 0.6-0.8 % breakage for three and nine bends. At high velocity, the breakage percentages were much more concentrated, lying between 6 and 7 % for both the three and nine bends. Greater difference between duplicates was seen in the nine bends than the three bends.

#### 4.1.4. Laser diffraction results of lignin from 12H, 22H, and 22V

Figs. 4.1.4.1, 4.1.4.2, & 4.1.4.3 below display the frequency charts of the post-pneumatically conveyed lignin particles in the 12 mm horizontal setup, the 22 mm horizontal setup, and the 22 mm vertical setup, respectively, under mild conditions (three bends, low velocity – red lines) and extreme conditions (nine bends, high velocity – green lines). The mild and extreme lignin PSD's are also matched up against the PSD of the original lignin pre-pneumatic conveying.

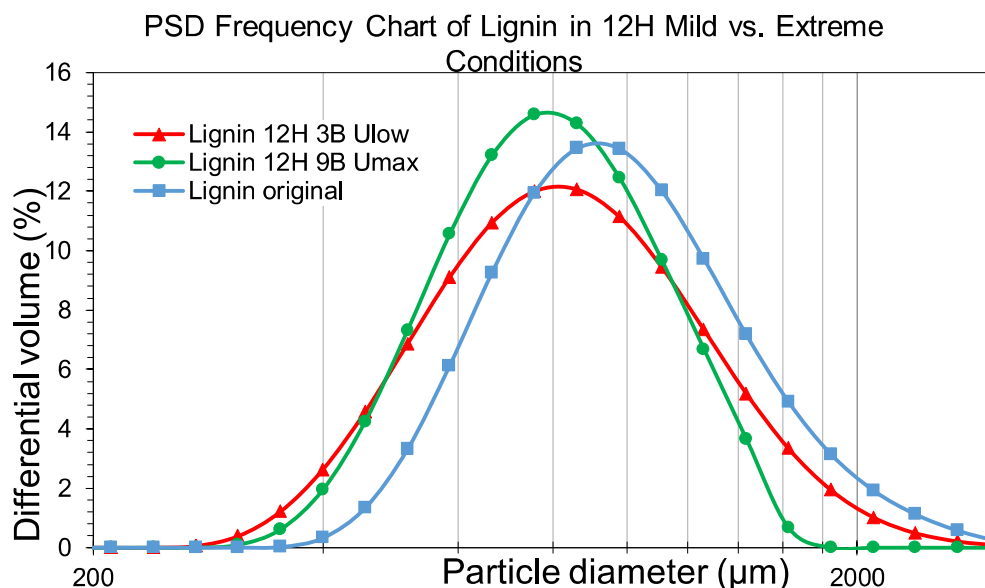
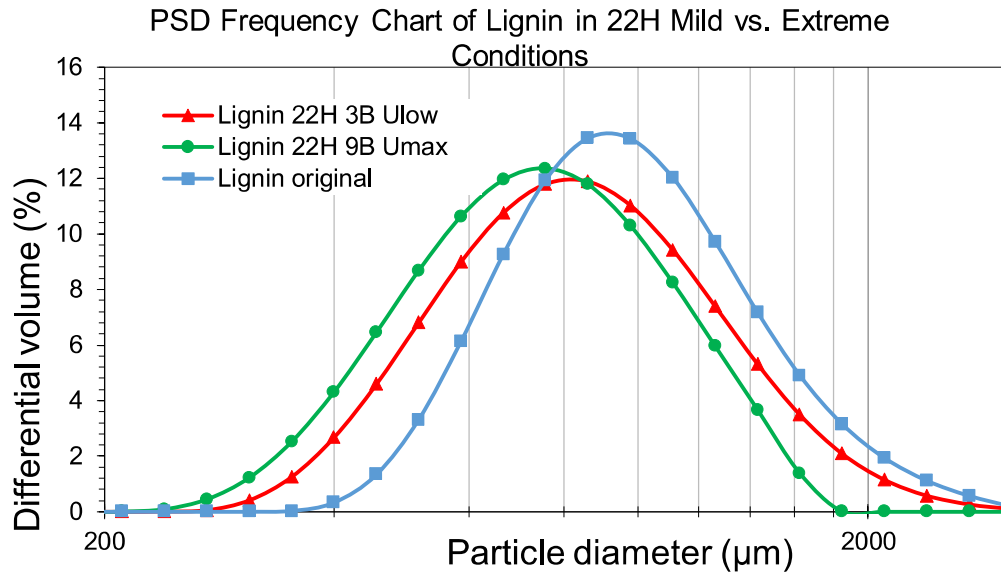


Fig. 4.1.4.1. Frequency chart for particles size distribution of lignin from 12 mm horizontal setup.

In Fig. 4.1.4.1, the lignin particles frequency distribution of the 12 mm horizontal setup is shown. The largest PSD is held by the original lignin particles (the blue line). At mild conditions (the red line), the PSD shifts to the left, meaning a smaller PSD than the original lignin's PSD. At extreme conditions (the green line), the breakage is even greater and so the green line is shifted slightly more to the left, which can be observed at the right bottom end of the green PSD.





Frequency Fig. 4.1.4.2. chart for particles size distribution of lignin from 22 mm horizontal setup.

In Fig. 4.1.4.2, the lignin particles frequency distribution of the 22 mm horizontal setup is shown. The largest PSD is held by the original lignin particles (the blue line). At mild conditions (the red line), there is a shift to the left of the original lignin PSD, so the PSD of the mild condition lignin is smaller. Visually, the shift of the red line in Fig. 4.1.4.2 is similar to the one in Fig. 4.1.4.1. At the extreme conditions, there is an even further shift to the left indicating a smaller PSD. The green shift in Fig. 4.1.4.2 is greater than the green shift in Fig. 4.1.4.1.

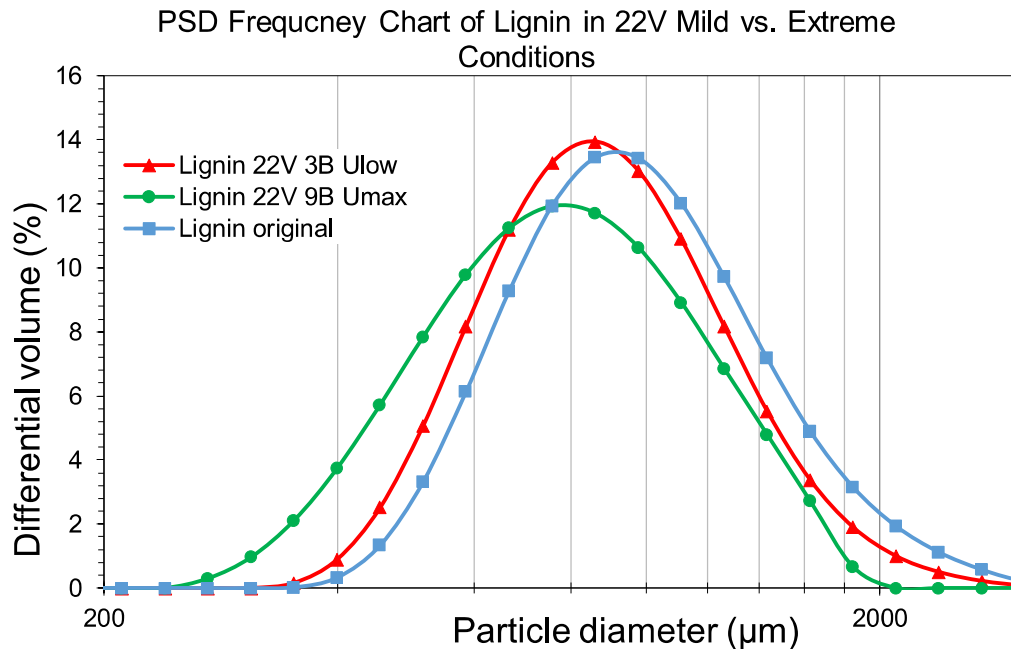


Fig. 4.1.4.3. Frequency chart for particles size distribution of lignin from the 22 mm vertical setup.

In Fig. 4.1.4.3, the lignin particles frequency distribution of the 22 mm vertical setup is shown. The largest PSD is held by the original lignin particles (the blue line). The PSD of the lignin particles at mild conditions (red line) shifts to the left of the original, meaning that the PSD of the mild lignin is smaller

than the one of the original lignin. The PSD of the extreme lignin (green line) shifts even further to the left, indicating that its PSD is even smaller than the mild lignin. Compared to the extreme lignin PSD in *Fig. 4.1.4.2*, the extreme lignin PSD in *Fig. 4.1.4.3* is slightly larger, with the maximum particle size being around 2000  $\mu\text{m}$ .

The laser diffraction results of the differential lignin PSD's show particular similarities among the different setups. The first one is that in all differential PSD charts (12 mm horizontal, 22 mm horizontal, and 22 mm vertical) the original lignin particles have the largest PSD. The mild lignin particles have the second largest PSD in all the setups. The extreme lignin particles have the smallest PSD in all the setups, since they are shift further to the left than the mild lignin PSD.

## 4.2. Cocoa Powder

Three sets of experiments were executed for the cocoa powder. The first set was done in the 12 mm (diameter) horizontal setup. In this set, two different number of bends (three bends and nine bends) were varied with 2 different velocities (9 m/s and 18 m/s). These were done to find out what the effects of **bend number** and **gas velocity** were. Thus, there were four experiments: (i) three bends, 9 m/s; (ii) three bends, 18 m/s; (iii) nine bends, 9 m/s; and (iv) nine bends, 18 m/s. These were duplicated resulting in a total of eight experiments for the 12 mm horizontal setup.

The second set was done in the 22 mm horizontal setup and the third was in the 22 mm vertical setup. Both these setups used three and nine bends as well as velocities of 9 m/s and 18 m/s just like the 12 mm horizontal setup. The 22 mm horizontal setup was created in order to find out what would happen if the **pipe diameter** of the conveying pipeline was increased. The 22 mm vertical setup was created in order to find out what would happen if the **orientation** of the conveying pipeline was changed.

Although the objective of the cocoa powder experiment was to "identify and quantify the agglomeration of cocoa powder after PC using laser diffraction", the following results also show yield (the percentage of cocoa powder that was successfully conveyed per experiment). The yield was used as a result because it was identified that there was always at least 10 % product loss in the pipeline and depending on the gas velocity, that loss could increase. Therefore, it was interesting to see whether this decrease in conveying yield was related to agglomeration (or if it even had anything to do with agglomeration).

#### 4.2.1. Cocoa Powder at Elevated Temperature

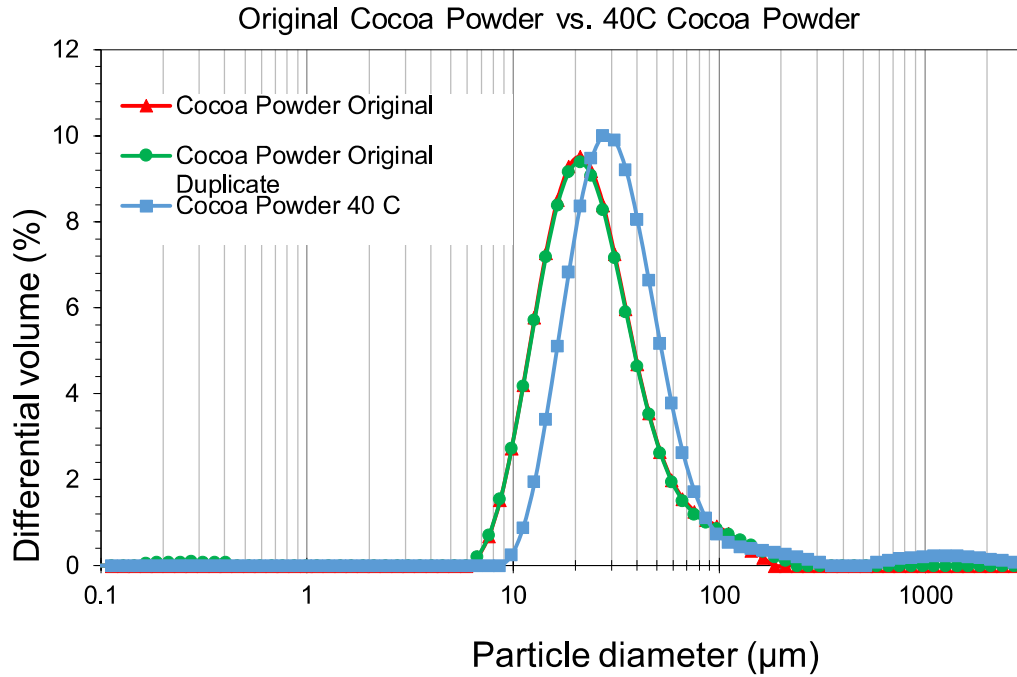


Fig. 4.2.1. Differential particle size distribution of original cocoa powder vs. cocoa powder left at 40°C for 15 minutes.

The first cocoa experiment was done by heating cocoa powder at 40°C for 15 minutes with the goal of checking for agglomeration. Fig. 4.2.1 shows the increase in particle size distribution of the heated cocoa powder. This proves that at increased temperature, agglomeration will occur to a certain extent. It is known that the lower melting point of cocoa lipids (on particle surface) is 25°C while the higher melting point where all cocoa lipids are molten is above 36°C (Petit et al., 2016). Based on the cocoa powder caking experiments of Petit et al. (2016), the highest caking indices were obtained by fatty cocoa powder (21 % fat) stored at 40°C. They reported that elevated temperatures and higher fat content contributed significantly to caking. Petit et al. (2016) observed an increase in particle size of their 21 %-fat cocoa powder and elucidated that the particle size increase probably resulted from the migration of fat towards the particle surface.

#### 4.2.2. 12 mm Horizontal Cocoa Yield

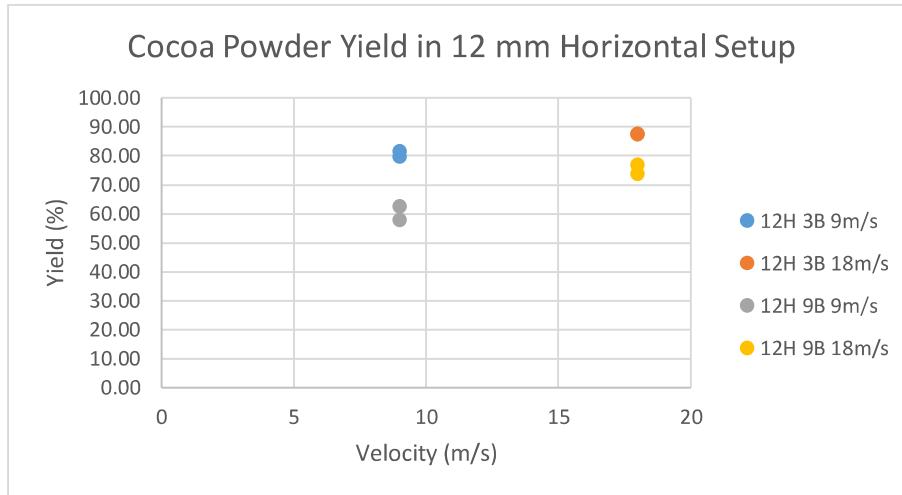


Fig. 4.2.2.1. Yield percentages of cocoa powder experiments in 12 mm horizontal setup.

Table 4.2.2.1. Yield values of 12 mm horizontal setup.

Exp name	Bends	Velocity (m/s)	Yield (%)
12H 3B 9m/s	3	9	81.59
	3	9	79.79
12H 3B 18m/s	3	18	87.78
	3	18	87.72
12H 9B 9m/s	9	9	62.59
	9	9	58.12
12H 9B 18m/s	9	18	73.76
	9	18	76.99

Fig. 4.2.2.1 shows that the average yield of the 18 m/s experiments is higher than the average yield of the 9 m/s experiments (around 11.04 %). This is mainly because there is more kinetic energy available to convey the cocoa powder mass, as can be described the kinetic energy equation:

$$E_k = \frac{1}{2} m (0.7 * V_{air})^2 * k \dots\dots\dots (Eq. 4.2.1)$$

$E_k$  is the kinetic energy in joules or kilojoules.  $m$  is the mass of the particle in kilograms.  $V_{air}$  is the gas velocity in m/s. In this equation, the velocity of the particle is needed. According to van Laarhoven (2010), the particle velocity is usually 0.7 times the gas velocity, so this value will be used.  $k$  is a coefficient for the number of bends – the assumption is that each bend equals one collision.

When comparing the yields based on the number of bends, the experiments with three bends always show a higher yield than the experiments with nine bends. This is valid for both the 18 m/s experiments and the 9 m/s experiments. This is mainly due to the lesser amount of resistance encountered by the cocoa particles when flowing through a setup with three bends instead of nine.

Fig. 4.2.2.1. also shows a larger yield decrease in the 9 m/s experiments (20.34 %) than in the 18 m/s experiments (12.38 %) when the number of bends is tripled (three bends to nine bends). This proves how much of an effect the velocity has on the conveying yield of materials.

When comparing the yield results between the three bend and the nine bend experiments, the nine bend experiments show slightly higher yield difference between their duplicates (4.47 % and 3.23 % for 9 m/s and 18 m/s respectively) than the three-bend experiments (1.8 % and 0.06 % for 9 m/s and 18 m/s respectively) – this can be calculated from *Table 4.2.2.1*. This is due to an increase in randomness for collisions and consequently sticking of cocoa powder on the pipeline wall or bends. If it is assumed that in each bend there is a maximum and minimum number of times a particle can interact with the wall or bend of the pipeline, then increasing the number of bends will result in a higher possibility for an increased number of particle-wall interactions. These interactions have an effect on the yield, and thus the yield values for experiments involving higher bend numbers have (slightly) greater difference. This agrees with the second law of thermodynamics that states that a system tends to progress in the direction of increasing entropy. Here, the system is the conveying pipeline combined with the air flow and cocoa powder while the entropy is randomness (Wang et al., 2016).

#### 4.2.3. 22 mm Horizontal Cocoa Yield

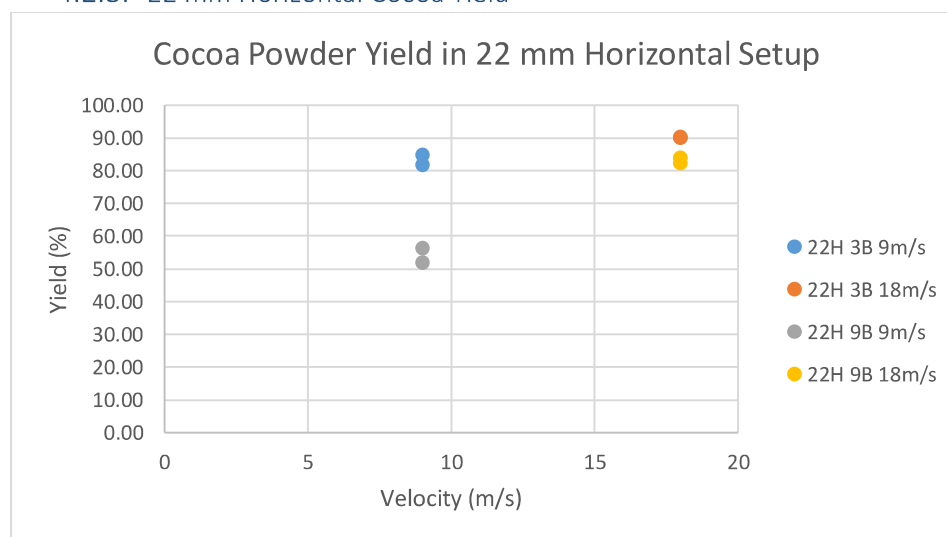


Fig. 4.2.3.1. Yield percentages of cocoa powder experiments in 22mm horizontal setup

Table 4.2.3.1. Yield values of 22 mm horizontal setup.

Exp name	Bends	Velocity (m/s)	Yield (%)
22H 3B 9m/s	3	9	84.72
	3	9	81.76
22H 3B 18m/s	3	18	90.30
	3	18	89.85
22H 9B 9m/s	9	9	56.14
	9	9	51.80
22H 9B 18m/s	9	18	82.10
	9	18	83.78

It can be seen in *Fig. 4.2.3.1* that the 18 m/s experiments have a higher average yield (86.51 %) than the 9 m/s experiments (68.61 %) – a 17.9 % decrease. This difference in average is caused by the drop in yield of the 9 m/s experiments (29.27 %) when the bends were tripled (three bends to nine bends) – the yield drop is 4.1 times larger than the yield drop of the 18 m/s experiments (7.14 %).

A noticeable occurrence in *Fig. 4.2.3.1* is that the yield values of the 22H 3B 9 m/s (blue circles) and 22H 9B 18 m/s (orange circles) are very similar – when taking the averages, they differ by only 0.3 %. This link [here](#) shows that for pneumatic conveying of coca powder in the 22 mm horizontal setup, if the velocity is doubled but the length of the pipeline is tripled, the yield values will be almost the same.

When looking at the duplicates of the experiments, the difference between yields of the three bends – 9 m/s and 18 m/s and nine bends – 9 m/s and 18 m/s experiments are 2.96, 0.45, 4.34, 1.68 %, respectively. It is clear that the experiments that used low velocities (9 m/s) have more difference in the duplicates than the high velocities. First of all, the difference in duplicates is caused by randomness of particle-wall collisions in the conveying system, assuming that all other parameters within a particular set of experiments are kept constant. In some runs, there are less particle-wall interactions and in some others there are more. With a higher velocity, there is more energy given to the particles. This extra energy makes up for the energy loss from the random particle-wall interactions (Borzzone et al., 1990), allowing the yield value to increase as if throughout the conveying line, there was only one impact per bend. In other words, the added energy from higher velocity overpowers the maximum possible energy loss from random particle-wall collisions.

*22 mm horizontal setup vs. 12 mm horizontal setup*

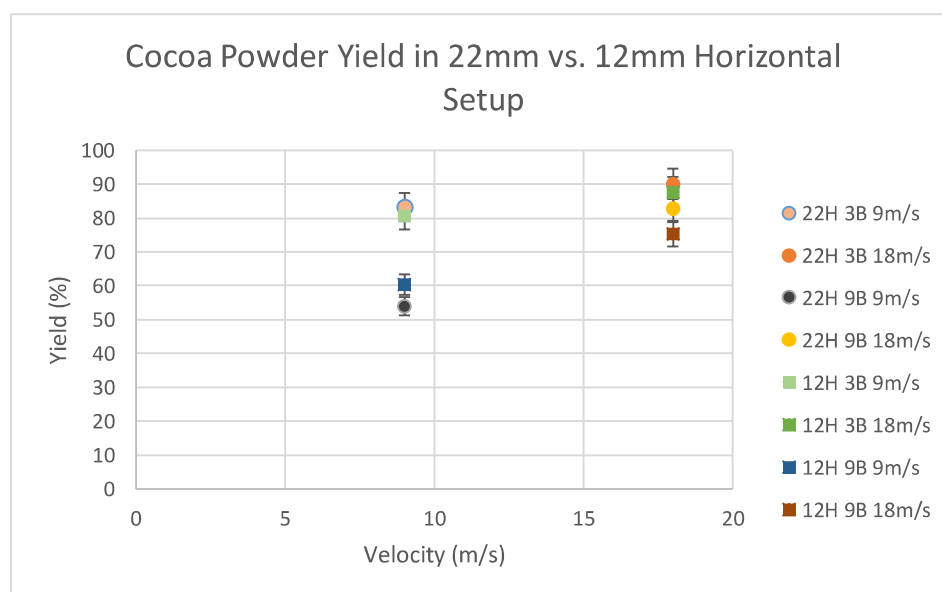


*Fig. 4.2.3.2. Plot of average yields from 22 mm horizontal and 12 mm horizontal setup experiments.*

*Table 4.2.3.2. Average yields of the 12 mm horizontal and 22 mm horizontal setups*

Exp name	Bends	Velocity (m/s)	Yield (%)
12H 3B 9m/s	3	9	80.69
12H 3B 18m/s	3	18	87.75
12H 9B 9m/s	9	9	60.36
12H 9B 18m/s	9	18	75.38
22H 3B 9m/s	3	9	83.24
22H 3B 18m/s	3	18	90.075
22H 9B 9m/s	9	9	53.97
22H 9B 18m/s	9	18	82.94

When compared to the yield results of the 12 mm horizontal setup, several things are noticeable (see Fig. 4.2.3.2). The first is that for the 18 m/s experiments, the 22 mm horizontal setup provided higher yields for the experiments with both three bends (90.08 vs. 87.75 %) and nine bends (82.94 vs. 75.38%). These values can be read in Table 4.2.3.2.

On the low velocity end (9 m/s), the 22 mm horizontal setup, three bends experiment is 2.55 % higher than the 12 mm, three bends experiment. Contrarily, when the bend number is tripled, (still on low velocity), the yield for the 22 mm horizontal setup is 6.39 % lower than the 12 mm setup. An increase of pipe diameter means less chance for particle-wall contact, but also causes more turbulence. By nearly doubling the pipe diameter, the particle-wall contact is decreased – this results in less resistance, less frictional forces, and higher yields. Due to increased turbulence, however, the yield increase is limited. In the 22 mm horizontal, 9 m/s experiments (three bends), turbulence is present, but since the setup is only three bends long, the turbulence doesn't have a significant effect on the yield and is overpowered by the "decreased particle-wall interaction", allowing the yield to be higher than in the 12 mm horizontal setup. In the 22 mm horizontal, nine bends experiment, even though the particle-wall interaction is less, the turbulence is still there. The effect of the turbulence is tripled (three bends to nine bends) and so it overpowers the "decreased particle-wall interaction". Therefore, the cocoa powder yield in the 22 mm horizontal, nine bends experiment (low velocity) is lower than in the 12 mm horizontal setup, nine bends.

#### 4.2.4. 22 mm Vertical Cocoa Yield

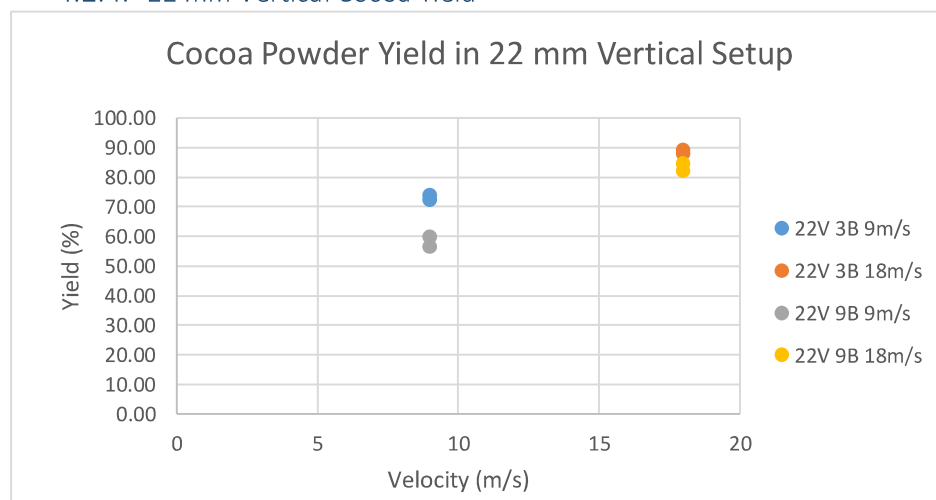


Fig. 4.2.4.1. Yield percentages of cocoa powder experiments in 22mm vertical setup

Table 4.2.4.1. Yield values of 22 mm vertical setup.

Exp name	Bends	Velocity (m/s)	Yield (%)
22V 3B 9m/s	3	9	74.15
	3	9	72.39
22V 3B 18m/s	3	18	88.03
	3	18	89.21
22V 9B 9m/s	9	9	60.13
	9	9	56.55
22V 9B 18m/s	9	18	82.24
	9	18	84.71

In Fig. 4.2.4.1, it can be seen that once again, the 18 m/s experiments have, on average, a higher yield (86.05 %) than the 9 m/s experiments (65.79 %). Also, all the yields of the 18 m/s experiments are above 80 %. At 9 m/s, there is roughly a 10 % drop in the yields when the bend number is increased from three bends to nine bends. In terms of the duplicates for each experiment type (bend number and velocity), there is a higher difference with the nine bend experiments (3.58 & 2.47 % for 9 m/s and 18 m/s, respectively) instead of the three bend experiments (1.76 & 1.18 % for 9 m/s and 18 m/s, respectively). This is due to the fact that with nine bends, the maximum number of possible collisions between the particle and the pipe wall increases. This results in a greater chance for larger differences to occur for the conveying yield.

#### 22 mm vertical setup vs. 22 mm horizontal setup

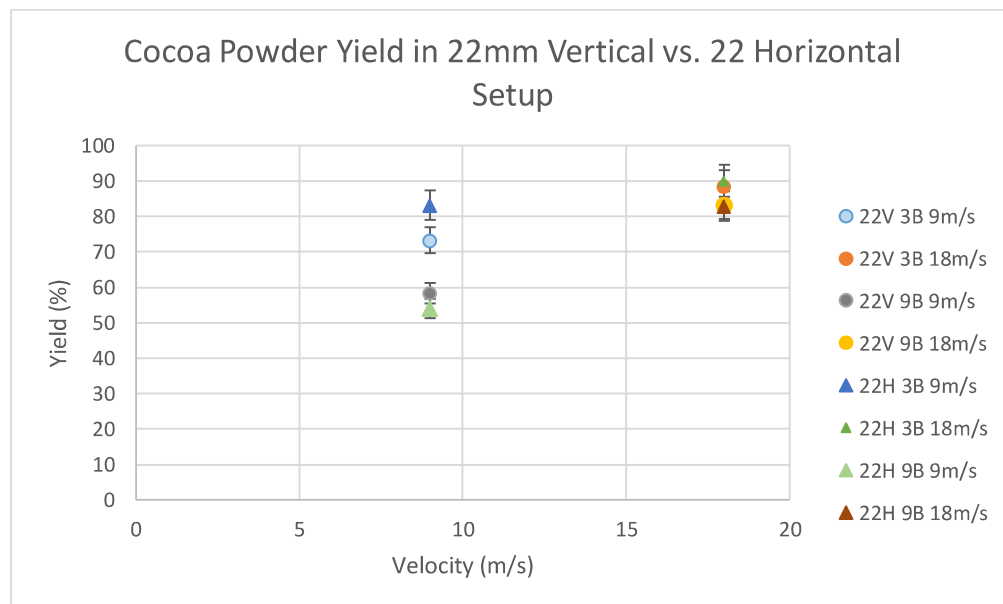


Fig. 4.2.4.2. Plot of average yields from 22 mm vertical and 22 mm horizontal setup experiments.

Table 4.2.4.2. Average yields of the 22 mm vertical and 22 mm horizontal setups

Exp name	Bends	Velocity (m/s)	Yield (%)
22H 3B 9m/s	3	9	83.24
22H 3B 18m/s	3	18	90.08
22H 9B 9m/s	9	9	53.97
22H 9B 18m/s	9	18	82.94
22V 3B 9m/s	3	9	73.27
22V 3B 18m/s	3	18	88.62
22V 9B 9m/s	9	9	58.34
22V 9B 18m/s	9	18	84.48

In Fig. 4.2.4.2, the highest yields originate from the three bend, 18 m/s experiments of the 22 mm horizontal and 22 mm vertical setups (the green triangle and orange circle, respectively). All the yields from the 18 m/s experiments from both the 22 mm horizontal and 22 mm vertical setups are above 80 % and remain concentrated within the 80 to 90 % range. This demonstrates that in the 22 mm diameter pipes, if the velocity is high enough (18 m/s), then the conveying yields will be somewhere between 80 and 90 %, no matter the orientation of the pipeline, nor the number of bends. The only yield above 80



% from the 9 m/s experiment is the one with three bends from the 22 mm horizontal setup (the blue triangle).

Interestingly, in the 9 m/s experiments, the 22H 3B yield (blue triangle) is around 83 %, 10 % higher than the 22V 3B yield (blue circle) and the 22H 9B (green triangle) is around 54 %, 4 % lower than the 22V 9B (grey circle). The higher yield of 22H 3B 9 m/s compared to the 22V 3B 9 m/s can be explained with pressure drop. It is known that pressure drop in vertical pipes is slightly higher than pressure drop in horizontal pipes (considering that a flow has been well-established in the horizontal pipe) because the weight of the air and solid particles has to be compensated ("Specificities of Vertical Pneumatic Conveying"; Argawal, 2005). In the vertical setup that was used, the setup was not one entirely vertical pipe, but rather a mix of vertically and horizontally oriented pipes. The reduction in yield, therefore, is caused by the combination of the already existing bends' decelerating effect on the gas and solids flow (Argawal, 2005) and having vertical pipes connected to horizontal pipes (like the number "five" on a digital clock).

At nine bends (still at 9 m/s), the 22H yield (green triangle) ends up 4.37 % lower than the 22V yield (grey circle). First of all, the low yields between 50 to 60 % are already the result of low velocity. At low velocity, the flow tends to be more laminar – that is the viscous forces dominate over inertia forces, dampening turbulence. The gas will flow in lines parallel to each other and the velocity profile would be that the further away from the wall, the higher the velocity. Maximum velocity is reached in the center of the pipe (Kamel & Shaqlaih, 2015). This could explain why the 22V yield (grey circle) is higher than the 22H yield (green triangle). In the horizontal pipe, at a certain velocity, a certain degree of saltation could occur, which can result in some settlement of product on the bottom of the pipeline. In the vertical pipe, choking could occur, where the particles would fall back on each other. The crucial part here is that the particles will fall back on the air stream and will not likely fall straight down on its "parallel line" of gas flow. Instead, it would fall back and perhaps shift and get picked up by other "velocity lines" which could be higher than the velocity line the particle was initially in. Due to this, particles in the vertical sections of the pipeline are more supported in terms of conveying ability rather than in the horizontal sections. In the 22 mm vertical setup, this "support" happens multiple times while in the 22 mm horizontal setup, the support doesn't take place at all since there are no vertical pipes in that setup. It is for this reason that the 22V yield is higher than the 22H yield. Still, the difference is only 4.37 % and the yield achieved by the 22V is only 58.34 %. This shows that the support provided by the vertical sections, although present, does not tremendously improve the conveying yield.

In contrast to the three bends experiments of the 22H and 22V (blue triangle and blue circle, respectively), the 22H yield is 9.97 % higher – more than double the difference at nine bends. This shows that the viscous effects of the air, the weight of the air and the weight of the solids are the leading cause of pressure drop in the 22V. The effect of the airflow support in the vertical sections are still present, but less apparent compared to the aforementioned effects. It is only when the pipeline is lengthened that the support from the up-flowing gas is visible.

From these cocoa powder pneumatic conveying experiments, it can be said that when the length – and thus bend number – of the conveying pipeline is minimized (three bends) and a high velocity (18 m/s is used), the conveying yield can reach up to 87-90 %. This is valid for the 12 mm horizontal, 22 mm horizontal, and 22 mm vertical setups. However, at low velocity (9 m/s) and with a high number of bends, that conveying yield drops to an average of around 60 % in the 12 mm horizontal and 22 mm vertical setups. In the 22 mm horizontal setup, it's around 53 %.

#### 4.2.5. Laser diffraction results of cocoa from 12H, 22H, and 22V

For the analysis of the cocoa powder particles, laser diffraction was used. The graphs used below are differential graphs, which show the particle size distribution (PSD) of particles that were successfully

conveyed (post-PC) and that remained in the pipe (in-pipe). They were further compared to the particle size distribution of the as-received cocoa powder. The laser diffraction results of the 12 mm horizontal setup, 22 mm horizontal setup and the 22 mm vertical setup can be seen in *Figs. 4.2.5.1, 4.2.5.2, and 4.2.5.3*, respectively.

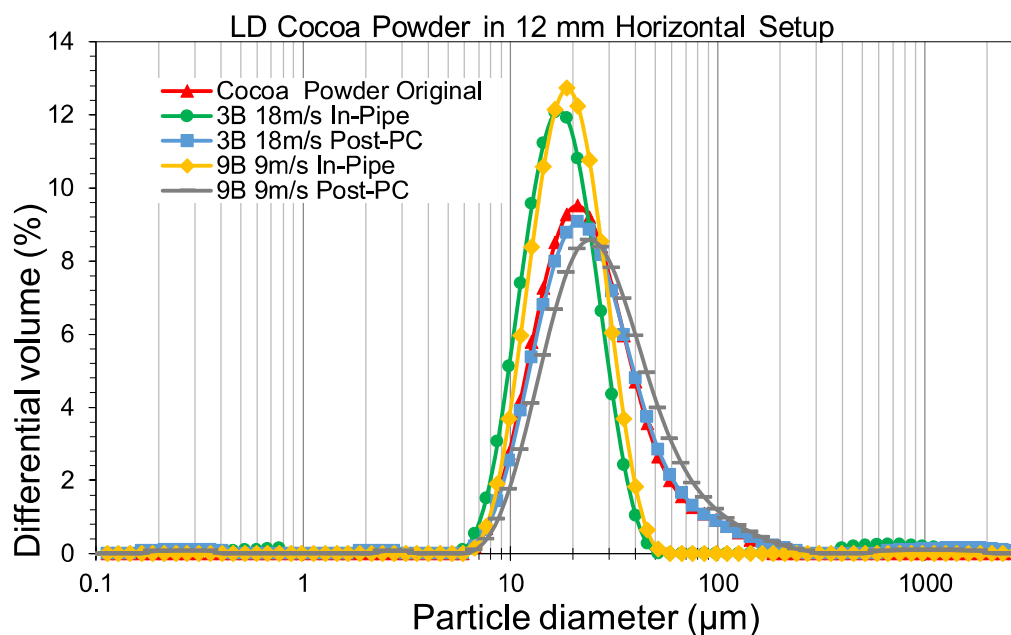


*Fig. 4.2.5.1. Differential particle size distribution of cocoa powder in the 12 mm horizontal setup at the extreme conditions compared to the original as-received material.*

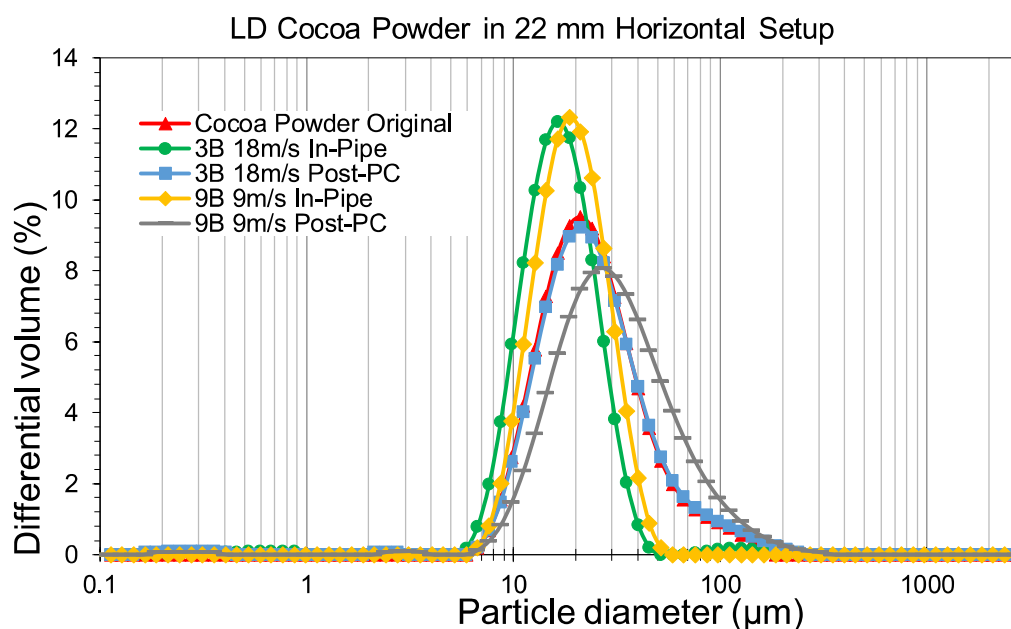


*Fig. 4.2.5.2. Differential particle size distribution of cocoa powder in the 22 mm horizontal setup at the extreme conditions compared to the original as-received material.*

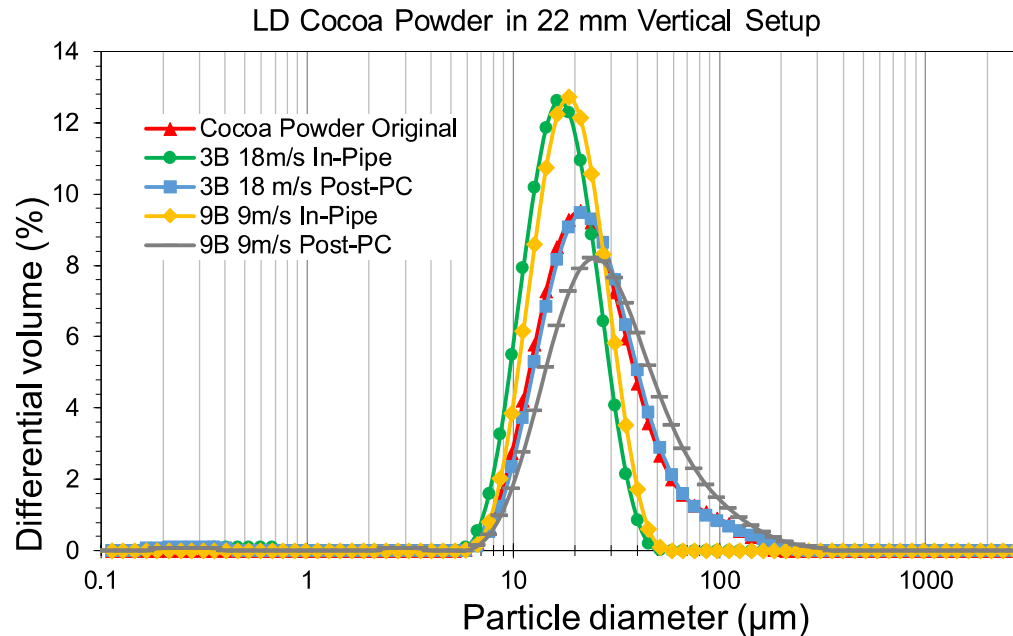


Fig. 4.2.5.3. Differential particle size distribution of cocoa powder in the 22 mm vertical setup at the extreme conditions compared to the original as-received material.

From Figs. 4.2.5.1, 4.2.5.2, & 4.2.5.3 it can be seen that the yellow and green lines represent in-pipe cocoa powder, the blue and grey lines represent the post-PC cocoa powder, and the red line is the as-received (original) cocoa powder. These figures use the laser diffraction values from the three bends, 18 m/s and nine bends, 9 m/s experiments in order to explain the maximum and minimum yields obtained in the sub-chapters 4.2.4, 4.2.3, and 4.2.2, above.

The first thing that can be said from Figs. 4.2.5.1, 4.2.5.2, & 4.2.5.3 is that in all the setups, the in-pipe cocoa powder (green and yellow lines) have similar particle size distributions (PSD) even though their conveying conditions achieved vastly different conveying yields (three bends, 18 m/s  $\approx$  90 % yield; nine bends, 9 m/s = 50–60 % yield). Moreover, their PSD's are always smaller than the PSD of the original cocoa powder (red line). It appears that no matter the conveying condition, the cocoa particles that remain in the pipe will have PSD's similar to each other and have PSD's smaller than the original cocoa powder. This could have been caused by the interaction between the surface lipids in the cocoa particles and pipeline wall. When the cocoa particles make impact with the pipeline wall, friction is produced, causing a slight increase in temperature. This melts the surface lipids of the cocoa particles and allows them to stick on the insides of the pipe. Measuring the extent of in-pipe sticking is limited to the collector, since there is a filter that could get clogged over time, resulting in pressure drop. This pressure drop makes it more difficult for conveying through the pipeline, meaning less material can get through and eventually, through this continuous cycle, pipeline blockage occurs.

The PSD of the three bend, 18 m/s post-PC cocoa powder (blue line) is nearly identical with the original cocoa powder in all setups. This pneumatic conveying condition achieved the maximum yield (average of 90 %) for all setups. The reason why the three bend, 18 m/s post-PC cocoa powder could have a similar PSD as the original cocoa powder could have been because the setup itself limits the interaction the cocoa powder has with the conveying pipeline – the residence time is very short. Three bends means minimum number of possible collisions while the gas velocity of 18 m/s allows the cocoa powder to travel through the pipeline in a split-second. This quick and limited-impact transportation contributed to the three bend, 18 m/s post-PC cocoa powder PSD to be almost the same as the original cocoa powder.

Finally, the PSD of the nine bend, 9 m/s post-PC cocoa powder (grey line) is the largest among all the cocoa powder PSD's in all setups. This conveying condition obtained the lowest yield from all the setups – around 50–60 %. The residence time of the cocoa powder in the pipeline is much longer and moreover, the number of collisions between the cocoa particles and pipeline wall are greater – there is more interaction. The halved gas velocity means that the cocoa particles are travelling slower and the extent of particle dilution is less than when the gas velocity was 18 m/s. Since they are less diluted, the particles are closer together and there is a higher chance of particle-particle interaction. When this is combined with the presence of nine bends, the increased number of collisions and already closer-packed particles generated more particle-particle interaction, which is why at the end, the cocoa particles that were successfully conveyed had a larger PSD than the as-received cocoa powder.

From the laser diffraction results of the cocoa powder differential PSD's, several things can be observed. This first is that in the 12 mm horizontal, 22 mm horizontal, and 22 mm vertical setups, the in-pipe cocoa powder (green and yellow lines) always has a smaller PSD than the original cocoa powder, no matter the conditions used. When using the conditions that provide high conveying yield – three bends, 18 m/s (blue line) – the post-PC PSD lines up almost perfectly with the PSD of the original cocoa powder (red line). And at nine bends and gas velocity of 9 m/s (low conveying yield conditions – grey line), the PSD of the post-PC cocoa shifts to the right – it is larger than the PSD of the original cocoa.

### 4.3. Rubber Particles

Six experiments were executed for the rubber particles. The first three experiments used the most extreme conditions while the second three experiments used the mildest conditions. The reason for this was to make identification of the different effects easier, since the parameters used were on the far ends of the "mild-to-extreme" scale. *Table 4.3.1* provides the list of experiments that were done. Here,  $U_{max}$  and  $U_{low}$  are the velocities which are 18 m/s and 9 m/s respectively. For the extreme conditions, the rubber particles were pneumatically conveyed multiple times – 20 runs, while the rubber particles in the mild conditions were only pneumatically conveyed once. B is the number of bends. After pneumatic conveying, the samples were analyzed with the Morphologi G3S to identify and quantify the particles' shape distribution. The shape parameters used for the analysis were circularity, convexity, and elongation.

*Table 4.3.1. Extreme and mild conditions used for the rubber particle experiments.*

Setup	Experiments with Extreme Conditions	Experiments with Mild Conditions
12 mm horizontal	9B; $U_{max}$ * 20 runs	3B; $U_{low}$ * 1 run
22 mm horizontal	9B; $U_{max}$ * 20 runs	3B; $U_{low}$ * 1 run
22 mm vertical	9B; $U_{max}$ * 20 runs	3B; $U_{low}$ * 1 run

#### 4.3.1. Original/As-received rubber particles

*Figs. 4.3.1.1, 4.3.1.2, & 4.3.1.3*, show the undersize distributions of the as-received rubber particles in terms of their circularity, convexity, and elongation (CCE), respectively. Circularity is how close a shape resembles a circle with the value 1 meaning the shape is a perfect circle. Convexity is how rough or spiky a particle is with the value 1 meaning the particle completely smooth. Elongation is one minus the aspect ratio. A particle that is symmetrical in all axes such as a square or a sphere has an elongation value of 0. There are two lines in each undersize chart because they are duplicates of the original rubber. Below each graphs are the mean values for the parameters that will be discussed for the first sample and the second sample.

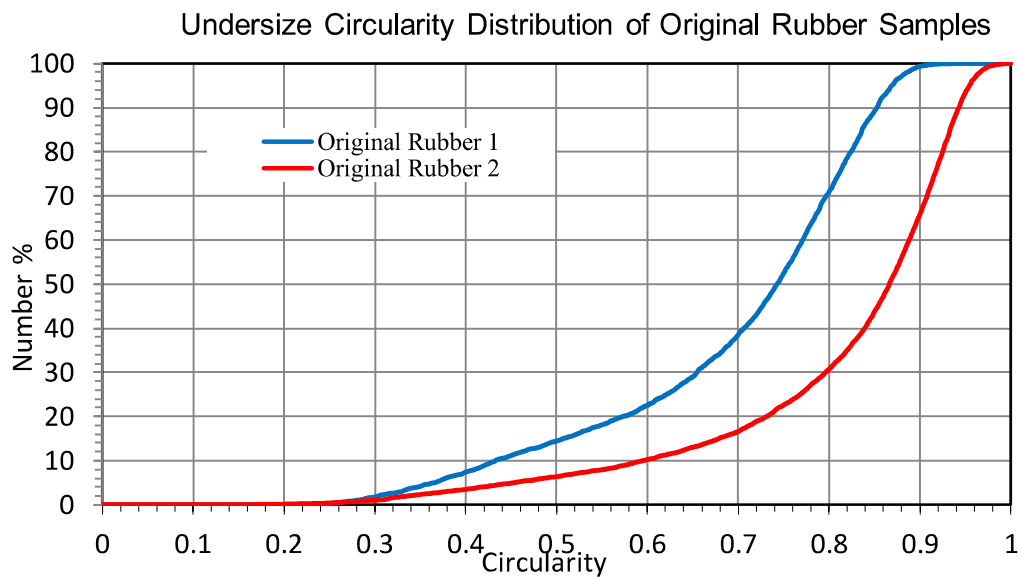


Fig. 4.3.1.1. Undersize particle shape distribution (circularity) of original rubber particles.

- 1 Mean Circularity Value Sample 1: 0.70
- 2 Mean Circularity Value Sample 2: 0.82

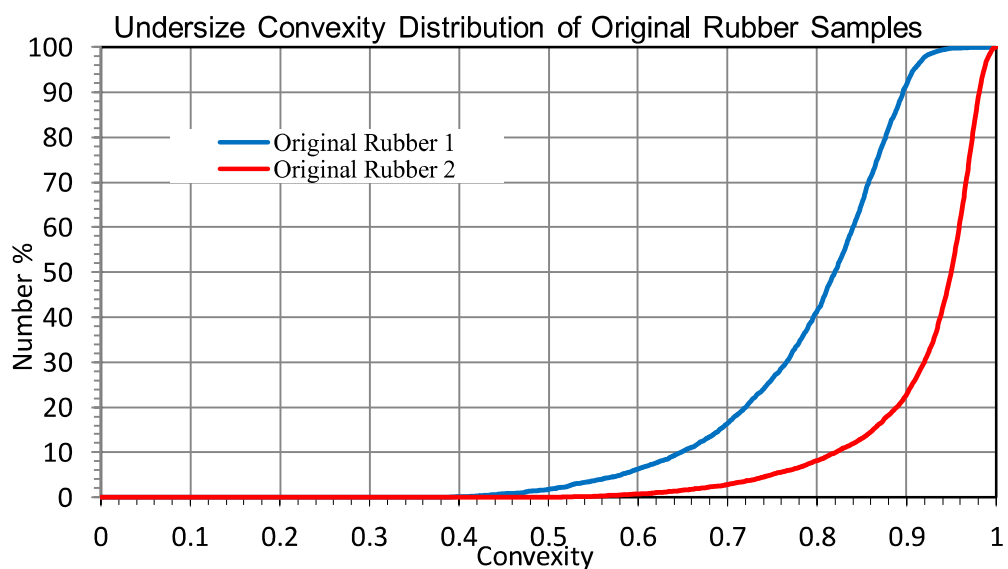


Fig. 4.3.1.2. Undersize particle shape distribution (convexity) of original rubber particles.

- 1 Mean Convexity Value Sample 1: 0.79
- 2 Mean Convexity Value Sample 2: 0.92

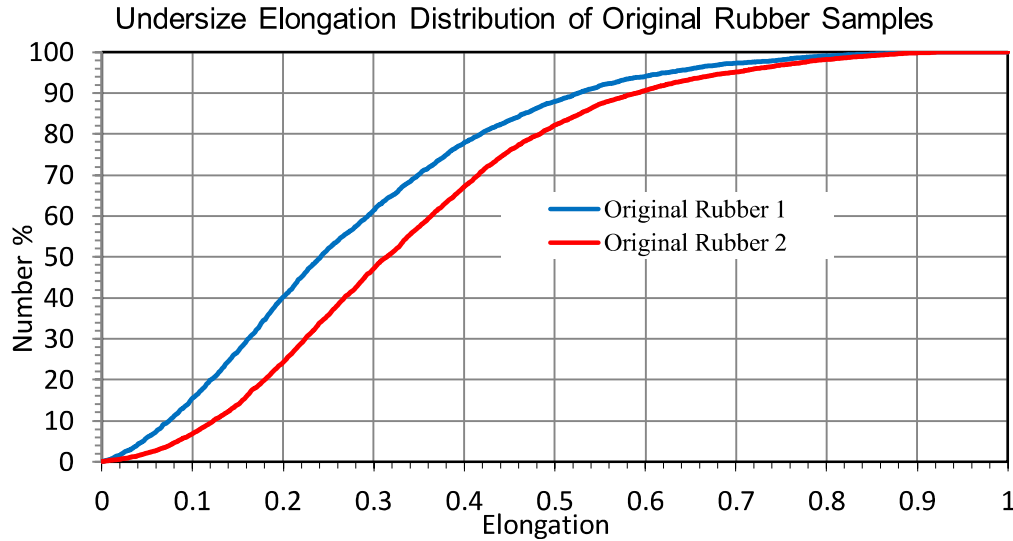


Fig. 4.3.1.3. Undersize particle shape distribution (elongation) of original rubber particles.

- 1 Mean Elongation Value Sample 1: 0.28
- 2 Mean Elongation Value Sample 2: 0.34

In Fig. 4.3.1.1, the difference in circularity mean value between the first original sample and the second original sample is 0.12. In Fig. 4.3.1.2, the difference in mean convexity values is 0.13 and in Fig. 4.3.1.3, the difference in mean elongation values is 0.06. Generally, based on these three charts, it can be said that the measurements of Original Sample 1 and Original Sample 2 for the circularity, convexity, and elongation are not repeatable due to their widely differing values, although the as-received material that was tested is the same. The most similar one is elongation. One reason why the measurements aren't accurate is because there weren't enough rubber particles to be measured. Each measurement was done with a few hundred particles, quite possible less. Normally, for the Morphologi G3S, tens of thousands of particles could be measured. Since these "few hundred particles" per measurement were taken from a jar of rubber particles, the samples taken for the measurements then were not representative of the whole rubber material and for example in Fig. 4.3.1.1, the first measurement (blue line) had a (much) lower circularity value than the duplicate measurement (red line). These two lines, in this case, can give a sense of variation present in the rubber particles for CCE.

#### 4.3.2. 12 mm Horizontal Setup (Original vs. Extreme vs. Mild)

The benchmark material, original rubber samples 1 and 2 (from Figs. 4.3.1.1, 4.3.1.2, & 4.3.1.3), were averaged and that averaged value for the CCE was used for the graphs below. This average value was compared to the analyses of the rubber particle CCE values obtained from the 12 mm horizontal setup experiments – both extreme and mild conditions. Extreme conditions were nine bends, 18 m/s gas velocity, and 20 runs (or 20 times nine bends). Mild conditions were three bends, 9 m/s gas velocity, and 1 run (or 1 times three bends). It is taken into account that although the average is used, there is a difference of a few hundredths to a few tenths of a unit between the averaged original sample (averaged original) and what the values actually are.

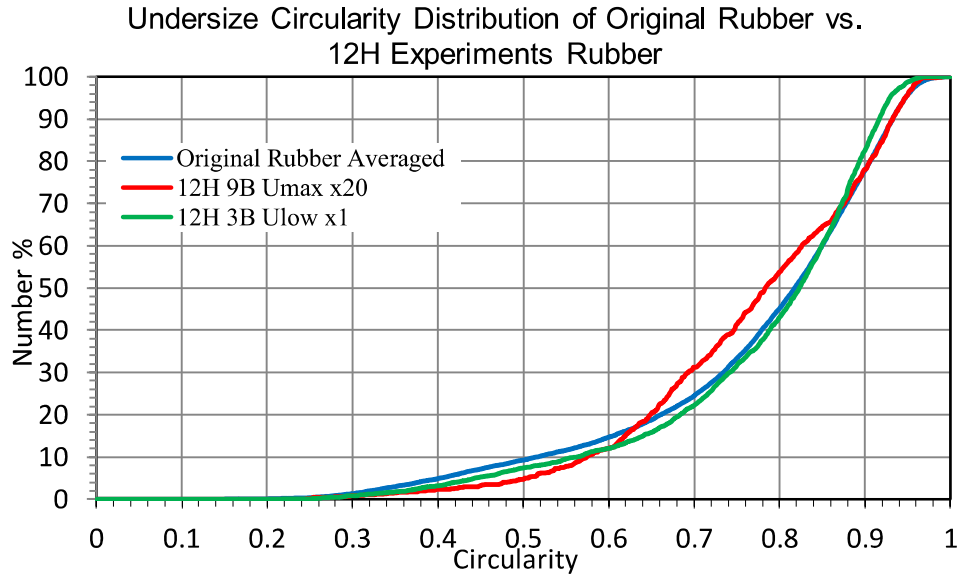


Fig. 4.3.2.1. Undersize particle shape distribution (circularity) of original rubber particles vs. 12H Extreme vs. 12H Mild.

- 1 Mean Circularity Value Combined Original (Blue line): 0.77
- 2 Mean Circularity Value 12H Extreme (Red line): 0.77
- 3 Mean Circularity Value 12H Mild (Green line): 0.78

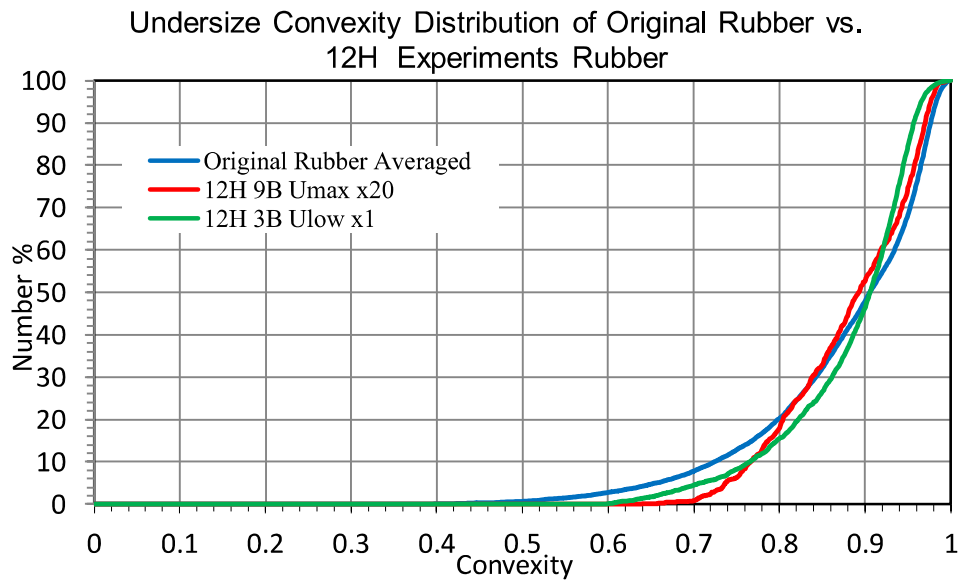


Fig. 4.3.2.2. Undersize particle shape distribution (convexity) of original rubber particles vs. 12H Extreme vs. 12H Mild.

- 1 Mean Convexity Value Combined Original (Blue line): 0.88
- 2 Mean Convexity Value 12H Extreme (Red line): 0.88
- 3 Mean Convexity Value 12H Mild (Green line): 0.88



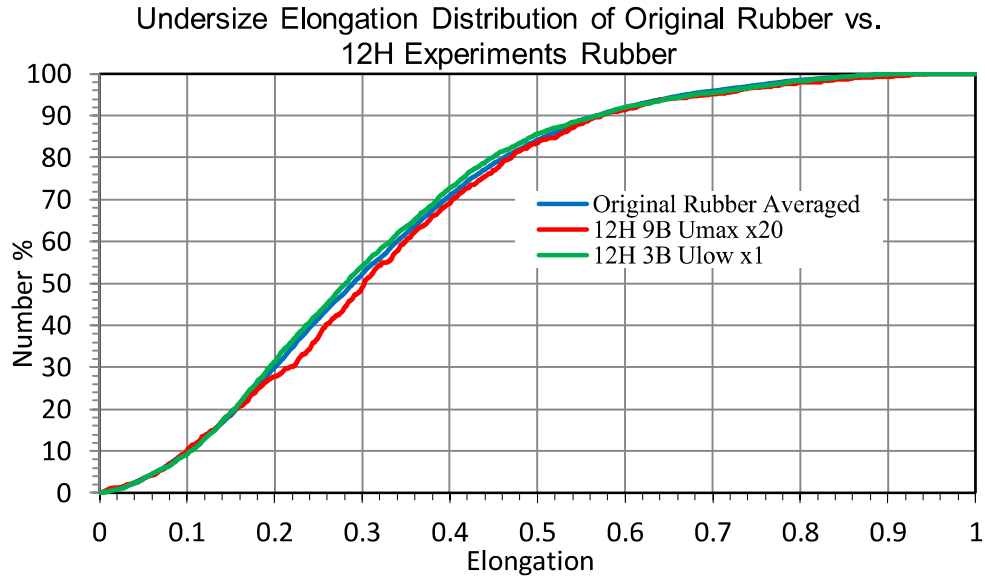


Fig. 4.3.2.3. Undersize particle shape distribution (elongation) of original rubber particles vs. 12H Extreme vs. 12H Mild.

- 1 Mean Elongation Value Combined Original (Blue line): 0.317
- 2 Mean Elongation Value 12H Extreme (Red line): 0.327
- 3 Mean Elongation Value 12H Mild (Green line): 0.312

Fig. 4.3.2.1 shows the comparison of circularity undersize distribution of the combined (averaged) original sample (blue line), the 12H extreme sample, and the 12H mild sample. They are very similar and have identical mean values – they red and green lines follow the blue line very closely, nearly overlapping. If this is compared to Fig. 4.3.1.1, then it can be seen that the 12H extreme and mild circularity values lie within the circularity range of the original samples 1 and 2.

When looking at Figs. 4.3.2.2 & 4.3.2.3, the same can be said: the convexity (Fig. 4.3.2.2) and elongation (Fig. 4.3.2.3) values of the 12H extreme and 12H mild experiments almost perfectly overlap with the averaged original convexity and elongation values. Due to the fact that the undersize distribution lines of the CCE values of the 12H extreme and 12H mild experiments follow the averaged original CCE values so closely, the conclusion that can be drawn is: the 12H extreme and mild experiments did not change the rubber particles at all. The slight variation (around 0.01 to 0.1 units) between the CCE values of the averaged original and the 12H extreme and 12H mild may be the result of sampling.

#### 4.3.3. 22 mm Horizontal Setup (Original vs. Extreme vs. Mild)

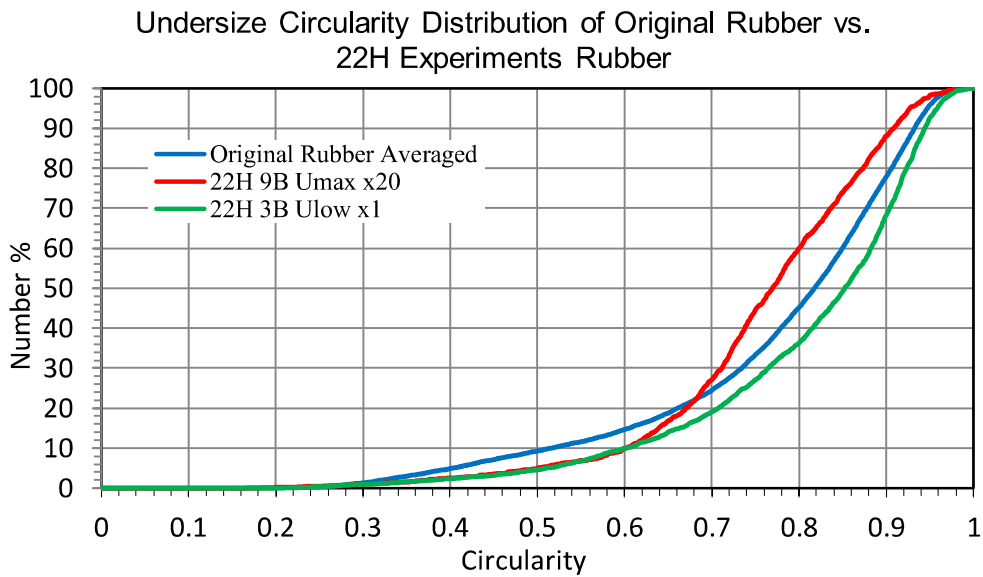


Fig. 4.3.3.1. Undersize particle shape distribution (circularity) of original rubber particles vs. 22H Extreme vs. 22H Mild.

- 1 Mean Circularity Value Combined Original (Blue line): 0.77
- 2 Mean Circularity Value 22H Extreme (Red line): 0.76
- 3 Mean Circularity Value 22H Mild (Green line): 0.81

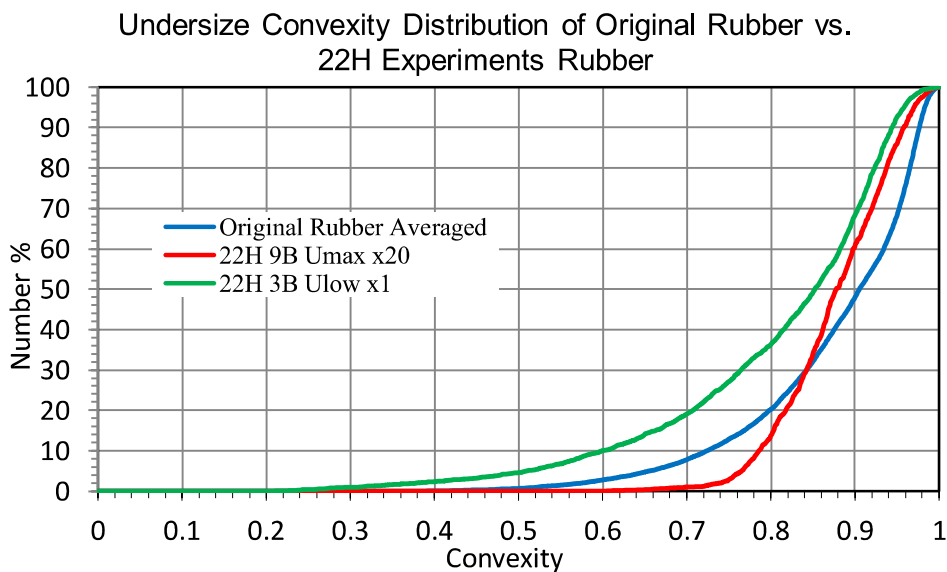


Fig. 4.3.3.2. Undersize particle shape distribution (convexity) of original rubber particles vs. 22H Extreme vs. 22H Mild.

- 1 Mean Convexity Value Combined Original (Blue line): 0.88
- 2 Mean Convexity Value 22H Extreme (Red line): 0.88
- 3 Mean Convexity Value 22H Mild (Green line): 0.92

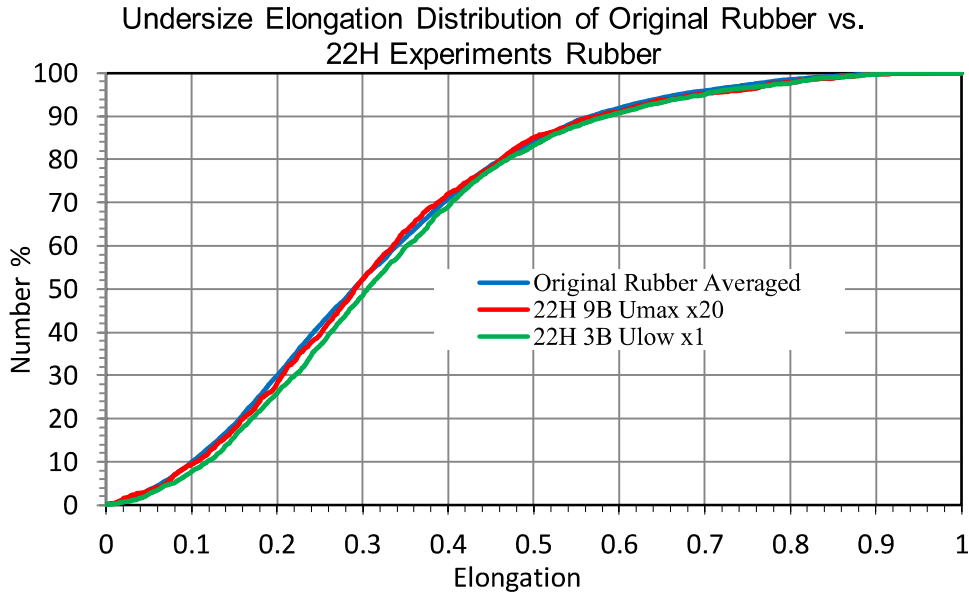


Fig. 4.3.3.3. Undersize particle shape distribution (elongation) of original rubber particles vs. 22H Extreme vs. 22H Mild.

- 1 Mean Elongation Value Combined Original (Blue line): 0.317
- 2 Mean Elongation Value 22H Extreme (Red line): 0.32
- 3 Mean Elongation Value 22H Mild (Green line): 0.332

Figs. 4.3.3.1, 4.3.3.2, & 4.3.3.3 present the comparisons undersize graphs for the CCE values between the averaged original rubber and rubber from the 22 mm extreme and mild experiments. It appears that only in Fig. 4.3.3.3 do the 22H extreme and mild lines (representing the undersize elongation distribution) follow the averaged original undersize elongation distribution very closely, nearly perfectly overlapping. Figs. 4.3.3.1 & 4.3.3.2 show a greater difference than compared to Fig. 4.3.3.3. Although this is the case, if Figs. 4.3.3.1 & 4.3.3.2 are compared to Figs. 4.3.1.2 & 4.3.1.3 (un-averaged, undersize distribution for circularity and convexity of the original rubber, respectively), then the variation in circularity and convexity values within Figs. 4.3.3.1 & 4.3.3.2 lie within the range of the original rubber particles. In other words, the difference that was found in Figs. 4.3.3.1 & 4.3.3.2 could have been the result of the variation in the shape of the original rubber particles. Thus, not a strong conclusion could be made saying that one type of conveying setup (22H extreme or 22H mild) had a greater effect on one of the parameters (CCE).

#### 4.3.4. 22 mm Vertical Setup (Original vs. Extreme vs. Mild)

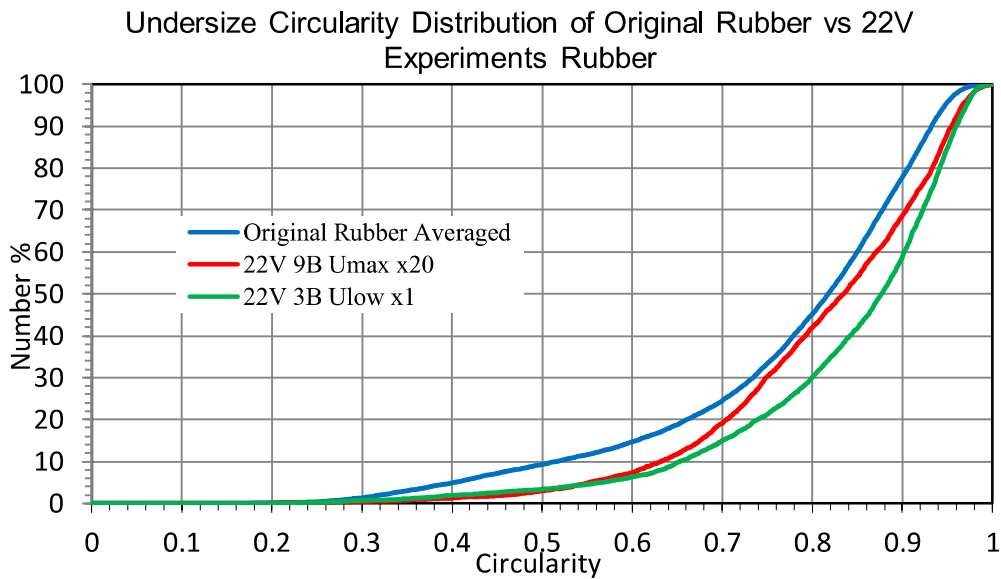


Fig. 4.3.4.1. Undersize particle shape distribution (circularity) of original rubber particles vs. 22V Extreme vs. 22V Mild.

- 1 Mean Circularity Value Combined Original (Blue line): 0.77
- 2 Mean Circularity Value 22V Extreme (Red line): 0.81
- 3 Mean Circularity Value 22V Mild (Green line): 0.84

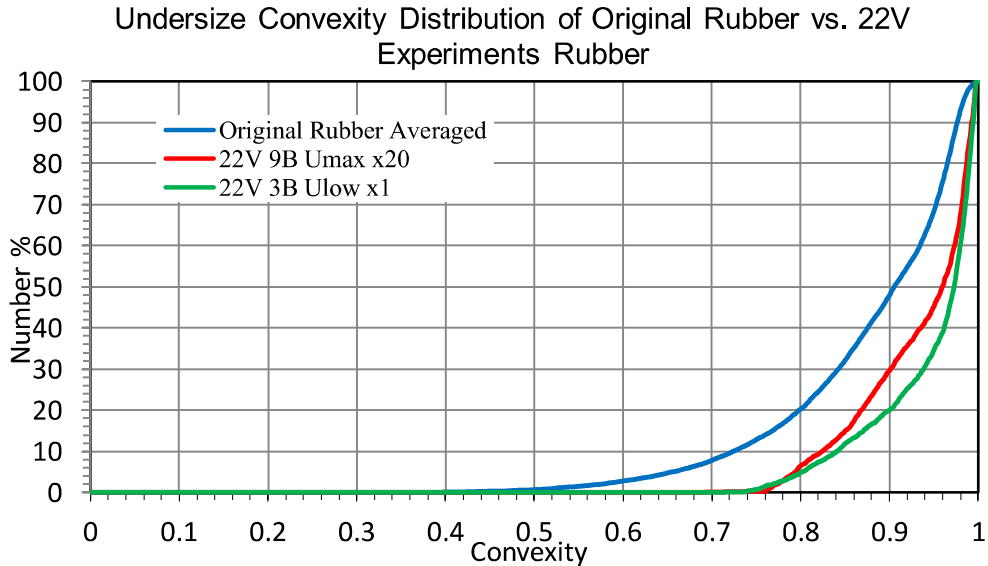


Fig. 4.3.4.2. Undersize particle shape distribution (convexity) of original rubber particles vs. 22V Extreme vs. 22V Mild.

- 1 Mean Convexity Value Combined Original (Blue line): 0.88
- 2 Mean Convexity Value 22V Extreme (Red line): 0.94
- 3 Mean Convexity Value 22V Mild (Green line): 0.96

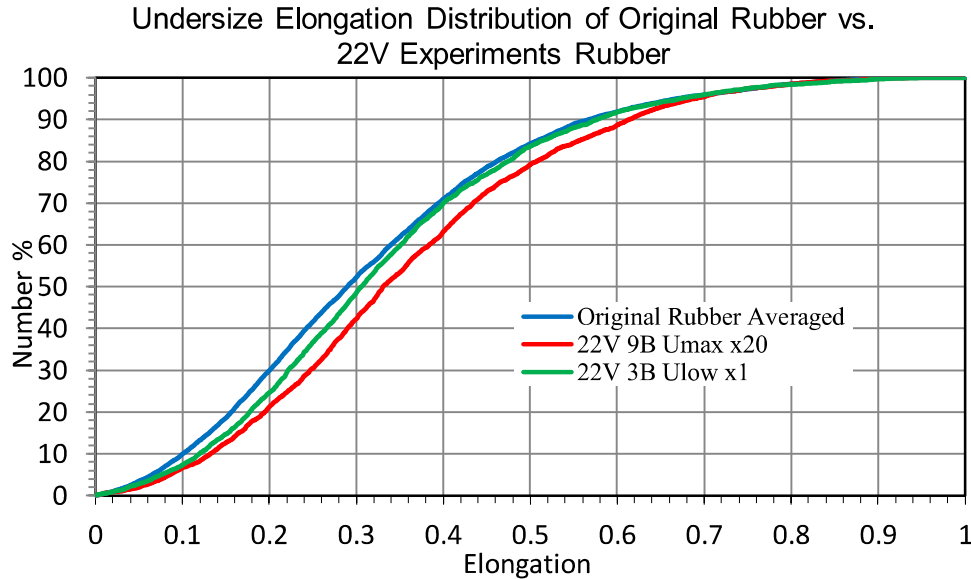


Fig. 4.3.4.3. Undersize particle shape distribution (elongation) of original rubber particles vs. 22V Extreme vs. 22V Mild.

- 1 Mean Elongation Value Combined Original (Blue line): 0.317
- 2 Mean Elongation Value 22V Extreme (Red line): 0.356
- 3 Mean Elongation Value 22V Mild (Green line): 0.331

Figs. 4.3.4.1, 4.3.4.2, & 4.3.4.3 display the undersize distribution charts of the original rubber particles vs. rubber particles from the 22V extreme and mild experiments of which the comparisons are of the circularity, convexity, and elongation values. In Fig. 4.3.4.1, the circularity distribution of the 22V mild experiment rubber particles (green line) deviates slightly more from the original rubber (blue line) than the extreme experiment rubber particles (red line). Although when compared to Fig. 4.3.1.1, the circularity undersize distribution of the 22V mild rubber is almost the same as the circularity undersize distribution of original rubber 2, with a difference of mean value of 0.02 units.

In Fig. 4.3.4.2, the undersize convexity (value of 1 means completely smooth) distribution graphs of the 22V extreme and 22V mild seem to increase compared to the averaged original rubber particles (blue line). This agrees with the chipping or abrasion process which reduces the "spikes" on a particle, making it smoother (van Laarhoven, 2010). When compared to Fig. 4.3.1.2, these undersize graphs lie just beyond the upper convexity undersize distribution chart of the original rubber particles. This could suggest that the 22V extreme and mild experiments increased the convexity of the rubber particles. The mild experiments (green line) gave a higher undersize distribution curve for convexity than the extreme experiments (red line). Although the mild rubber particles had a higher undersize distribution curve for convexity, it still closely resembled the undersize distribution curve of original rubber 2 in Fig. 4.3.1.2. It could have been that the rubber particles used for the 22V mild conditions was had parts on the particles that could have been easily "hit" off, making it slightly more convex at the end of the conveying.

Finally, in Fig. 4.3.4.3, it is observed once again that the elongation undersize distribution curves of the 22V extreme and mild experiments follow the elongation undersize distribution curve of the averaged original rubber particles, with differences within a few hundredths of a unit. In Fig. 4.3.4.3, the 22V extreme experiment rubber (red line) is shifted more to the right compared to the 22V mild experiments, and when compared to Fig. 4.3.1.3, the 22V extreme experiment rubber has a higher mean elongation value than the mean elongation value of original rubber 2 in Fig. 4.3.1.3 – the difference is 0.016 units. In the case of the elongation, the fact that the 22V extreme rubber has a higher elongation than the 22V mild rubber means that the experiment conditions agree with the acquired result – extreme condition

means higher overall kinetic energy which can cause greater deformation. The first thing that could have caused this is the high velocity (18 m/s). Every impact on the pipeline wall would technically be around four times greater if 18 m/s was used than if 9 m/s (based on the kinetic energy equation – Eq. 4.1.1). Then the difference in impact number: the mild conditions (three bends, 9 m/s times 1 run) would generally only have three collisions between the rubber particle and pipeline while the extreme conditions (nine bends, 18 m/s times 20 runs) would have 180 collisions. Rubber also has a friction coefficient of around 0.7 ("Friction and Automobile Tires"). It's mass and elasticity makes it bounce more frequently in the pipeline. All of these combined generate relatively more friction and thus more heat. Therefore, the chances that the 22V extreme rubber will be more elongated is higher. The orientation of the pipeline must have also played a role. See explanation in sub-chapter 4.1.3. On the contrary, this explanation implies that the shift in elongation should be much larger than what is portrayed in *Fig. 4.3.4.3*. That would mean that rubber particles are not easily affected by pneumatic conveying, even under extreme conditions, if it is indeed the pneumatic conveying system that caused this shift. Otherwise, it would only be, once again, the variation of particles from the original, pre-PC rubber.

#### 4.3.5. Comparison of All Setups (Original vs. Extreme Vs. Mild)

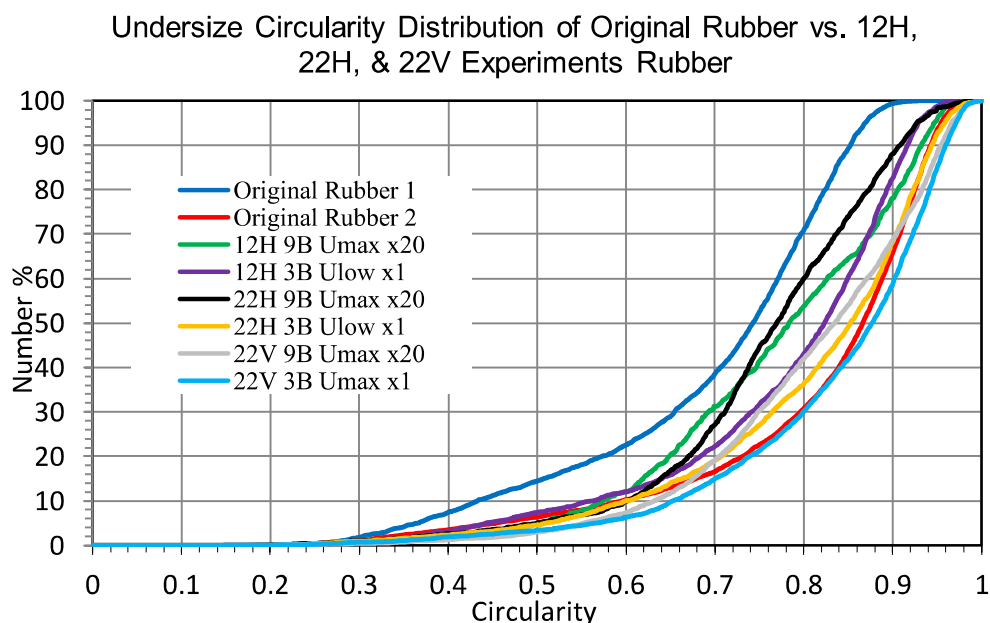


*Fig. 4.3.5.1. Undersize particle shape distribution (circularity) of original rubber particles vs. 12H, 22H, & 22V extreme and mild experiments.*

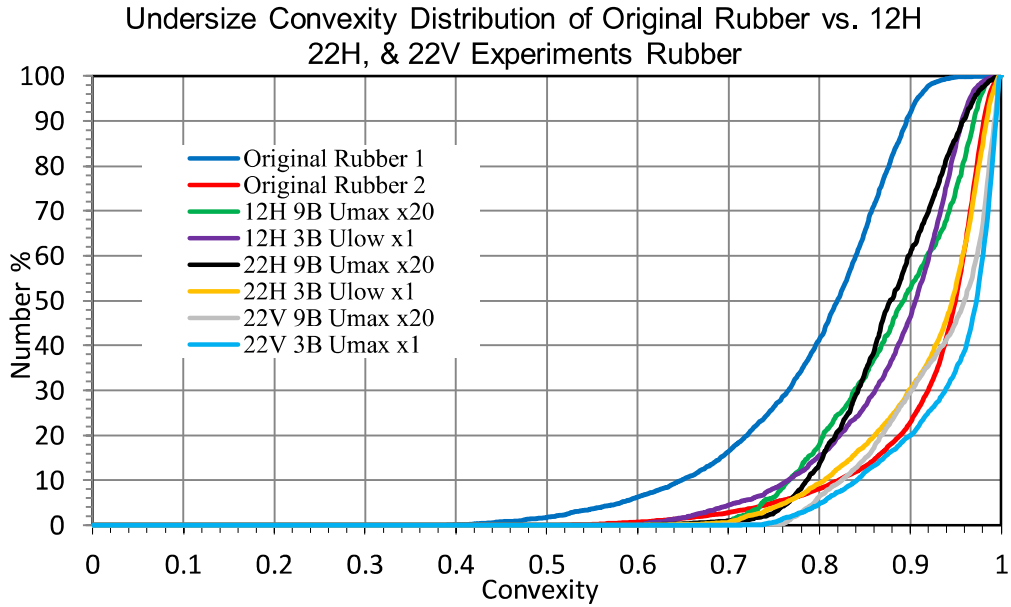


Fig. 4.3.5.2. Undersize particle shape distribution (convexity) of original rubber particles vs. 12H, 22H, & 22V extreme and mild experiments.

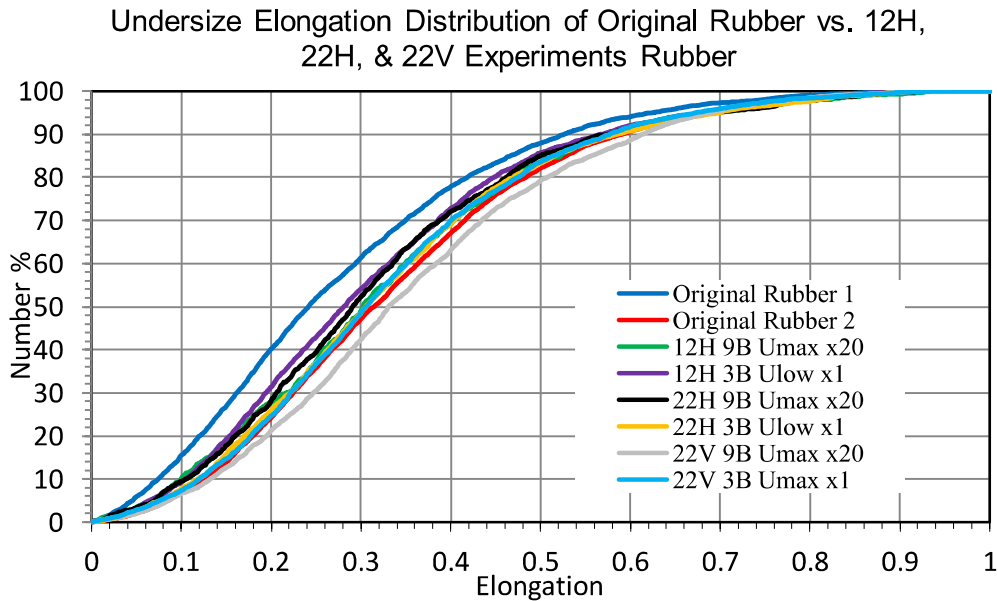


Fig. 4.3.5.3. Undersize particle shape distribution (elongation) of original rubber particles vs. 12H, 22H, & 22V extreme and mild experiments.

From Figs. 4.3.5.1, 4.3.5.2, & 4.3.5.3, it is noticeable that all the CCE undersize distribution lines of all the experiments tend to be closer the CCE undersize distribution line of the original rubber sample 2 (red line) instead of the original sample 1 (blue line). Furthermore, a majority of the CCE undersize distribution lines lie within the border of the undersize distribution lines of original sample 1 and original sample 2. One or two lines do travel a bit outside of the border, for example in Fig. 4.3.5.3, where the 22V extreme rubber (grey line) is charted just beyond (to the right) the original sample 2 (red line). With



the majority within the borders, however, and the fact that not thousands of rubber particles were sampled, it could very well be that these lines outside of the borders are only slight variations to the rubber particles' CCE values which weren't able to be taken into account during the sampling of the original rubber sample 1 and sample 2.

## 5. Conclusions

The main objective of this research was to identify and quantify the breakage of lignin particles (a fragile solid), the agglomeration of cocoa powder (a heat sensitive solid), and the deformation of rubber particles (a highly elastic solid). That was done by developing three setups based on the pipe diameter and orientation – 12 mm horizontal, 22 mm horizontal, and 22 mm vertical setups. In addition to that, the different bend numbers (three and nine) and different conveying velocities (low and high, exact value based on material conveyed) were employed.

Velocity plays a significant role in the breakage of lignin and its effects are directly related – the higher the velocity, the higher the breakage. This, however, depends also on the pipe diameter of the setup. At high velocity, 12 mm horizontal setup, the breakage is only around 1 %. In the 22 mm horizontal setup, the breakage becomes five to six times higher.

The breakage percentages also increase when more bends are added, however its effect is not as large as velocity. Moreover, with an increase in bend number, there is also an increase in difference between breakages of experiments, considering the fact that the same velocity and pipe diameter are used. The value of this difference grows with increasing velocity. When comparing *Fig. 4.1.1.1*, *4.1.2.1*, & *4.1.3.1*, the greatest difference was shown by the duplicates of the high velocity experiment with nine bends in the 22 mm horizontal setup (see *Fig 4.1.2.1*); the difference of that duplicate a little over 1 %.

When moving to a more industrial setting (larger pipe diameters), an increase in turbulence is observed and this can further exacerbate the breakage values as well as the variation between breakage values for a specific velocity. Finally, the orientation of the pneumatic conveying setup (horizontal vs. vertical) also influences the breakage percentage of lignin by affecting the direction of deflection of the particles as well as the forces that come with it. In the vertical setup, specifically when particles move upwards through a vertical pipe followed by a horizontal pipe, there is an added effect of gravity that increases breakage rates. This is proven by *Fig. 4.1.4.3* (the frequency particle size distribution chart of the 22 mm vertical setup), where the particle size distribution decreased the most, compared to the particle size distributions of the 22 and 12 mm horizontal setups, under extreme conditions.

Cocoa powder was found to be a difficult material to convey due to its cohesive properties, which is due to its high fat content (21%). At high velocities (18 m/s), more than 70 % of cocoa powder can be successfully conveyed, even with nine bends. This is true for all (12H, 2H, and 22V) setups. In the setups with larger pipe diameter (22 mm), at least 80 % can be successfully conveyed even with nine bends, if high velocity is used. The maximum possible conveying yield of cocoa powder is around 87-90 %, which is obtained with high velocity (18 m/s) and low number of bends (three bends). At low velocity (9 m/s), it is still possible to achieve a conveying yield of around 80 % if three bends are used except in the 22 mm vertical setup which achieved an average yield of only 73 %. High number of bends (nine) and low velocity (9 m/s) results in the worst yield for all three setups, ranging from 50 to 60 %. From the analysis of the frequency PSD of the cocoa particles, the particles that remained in the pipe actually had a smaller size distribution than the particles that were successfully conveyed. The cocoa powder that was successfully conveyed with minimum bends and high velocity had similar PSD as the original cocoa and the post-PC cocoa of low velocity and high bend-number conditions had the largest PSD.

Rubber particles were analyzed for their particle shape before and after pneumatic conveying. The parameters used were circularity, convexity, and elongation. The original rubber samples that were analyzed for their particle shape had widely differing undersize distributions for the circularity and convexity measurements and to a lesser extent, the elongation. The duplicates weren't repeatable. After

pneumatic conveying (PC) in the 12H, 22H, and 22V setups under extreme and mild conditions, there weren't any significant changes to the rubber particles as the post-PC rubber particles had undersize distributions for the above parameters that tended to stay within the margin of the original rubber particle measurements. Thus, for these sets of experiments, it can be said that the pneumatic conveying process, under the used system-designs and conveying conditions, perhaps had some effect on the rubber particles, but that is not very pronounced due to the wide variation already present in the duplicates of the as-received material.

## 6. Recommendations

During the execution of experiments to obtain the above conclusions, a few limitations were encountered. The limitations will be acknowledged in this part of the report and recommendations for future research will be provided.

The first limitation is related to the lignin experiments. During experiments, a sieve analysis had to be done. After sieving to quantify the breakage percentage, the fines had to be recollected and added to the unbroken lignin particles to be analyzed with laser diffraction. In this recollection process, some fines were lost. There were also some fines that stuck on the filter paper which could not be added to the unbroken lignin particles. These factors may have resulted in some slightly different particle size distributions than it could have been. The highest fraction of pneumatically conveyed lignin particles (five grams) that turn into fines is only seven percent, which is only 0.35 grams. Thus, for future research using lignin, a higher mass of lignin should be pneumatically conveyed, so that relatively more fines could be obtained, and the laser diffraction analysis for particle size distribution could be more accurate.

A limitation for the cocoa particles experiments was that a 20 m/s gas velocity could not be reached, although in literature it is found that dilute phase conveying uses gas velocities of around 20 m/s. The maximum conveying yield achieved was around 90 %. It is recommended to conduct the cocoa experiments in 22 mm diameter pipes or larger pipes and at higher velocities (25 m/s) and more bends. This should be done to see whether an increase in velocity could produce agglomerated cocoa, since in the conclusion, it was found that at high velocity and three bends, the yield was the highest and the PSD was similar to the original cocoa powder. Therefore, it is possible that at a certain, increased, velocity (still three bends), the post-PC cocoa could agglomerate.

Finally, the rubber experiment limitations have to do with the size of the rubber particles and the microscope abilities itself. Due to the size of the rubber particles, it was impossible to measure/analyze thousands of particles on the glass plate of the Morphologi G3S. This resulted in the inability to capture a truly representative sample of the rubber particles used for the pneumatic conveying experiments as well as the rubber particles after pneumatic conveying. This, of course, impacted the values of the shape parameters (circularity, convexity, and elongation) used to quantify whether the rubber particles deformed. A suggestion for future experiments with highly elastic materials is to use a material with a general particle size around 0.1 mm or less. Also, it is not recommended to use rubber particles because it can sustain very high impact forces or strain and still return to its original shape. If the future researcher still opts for rubber, then a higher velocity should be used. The use of polymeric materials as highly elastic materials would be best.

## References

1. Rhodes, M. *Introduction to Particle Technology*; John Wiley & Sons: Chichester, England, 1998.
2. Choking Velocity in pneumatic transport - Correlation of Punwani - PowderProcess.net [https://powderprocess.net/Pneumatic\\_Transport/Choking\\_Velocity.html](https://powderprocess.net/Pneumatic_Transport/Choking_Velocity.html) (accessed Jul 7, 2021).
3. Wagner, P. Selecting Elbows for Pneumatic Conveying Systems. *Chemical Engineering Prog* **2007**, 28–32.
4. Resources Safety; Health Queensland. Dust hazards in mining <https://www.business.qld.gov.au/industries/mining-energy-water/resources/safety-health/mining/hazards/dust> (accessed Jul 7, 2021).
5. Verma, R.; Agarwal, V. K.; Pandey, R. K.; Gupta, P. Erosive Wear Reduction for Safe and Reliable Pneumatic Conveying Systems: Review and Future Directions. *Life Cycle Reliab. Saf. Eng.* **2018**. <https://doi.org/10.1007/s41872-018-0055-7>.
6. Mills, D.; Jones, M. G.; Agarwal, V. K. *Handbook of Pneumatic Conveying Engineering*; Taylor & Francis: Philadelphia, PA, 2004.
7. Rhodes, M. *Introduction to Particle Technology*; John Wiley & Sons: Chichester, England, 2008.
8. Wilms, H. Basics of Pneumatic Conveying Systems Design. In *AchemAmerica International Congress on the Process Industries*; Zeppelin Systems USA, Inc.: Mexico City, 2002; pp 4–5.
9. Huber, N.; Sommerfeld, M. Modelling and Numerical Calculation of Dilute-Phase Pneumatic Conveying in Pipe Systems. *Powder Technol.* **1998**, 99 (1), 90–101.
10. Barbosa, P. R.; Seleglim, P., Jr. Improving the Power Consumption in Pneumatic Conveying Systems by a Daptive Control of the Flow Regime. *J. Braz. Soc. Mech. Sci. Eng.* **2003**, 25 (4), 373–377.
11. Purutyan, H.; Troxel, T. G.; Cabrejos, F. Propel Your Pneumatic Conveying System to Higher Efficiency. *Chem. Eng. Pro* **2001**, 42–55.
12. Hall, S. Pneumatic Conveying. In *Branan's Rules of Thumb for Chemical Engineers (Fifth Edition)*; Butterworth-Heinemann: Oxford, England, 2012; pp 244–256.
13. Alkassar, Y.; Agarwal, V. K.; Pandey, R. K.; Behera, N. Influence of Particle Attrition on Erosive Wear of Bends in Dilute Phase Pneumatic Conveying. *Wear* **2020**, No. 203594, 203594.
14. Ortega-Rivas, E. *Unit Operations of Particulate Solids: Theory and Practice*; CRC Press: London, England, 2017.
15. SOLUTIONS for Pneumatic Conveying - palamatic process - PDF catalogs <https://pdf.directindustry.com/pdf/palamatic-process/solutions-pneumatic-conveying/108097-826103.html> (accessed Jul 7, 2021).
16. Nowak, S. Dense Phase Conveying. *Power Handling Solutions* **2017**, 6–11.
17. Mills, D. A Quick Check Method for The Design Of Pneumatic Conveying System. *Advances in Dry Processing* **2002**, 7–17.
18. Nowak, S. Vacuum conveying in the pharmaceutical industry <https://www.pharmtech.com/view/vacuum-conveying-pharmaceutical-industry> (accessed Jul 7, 2021).
19. Nowak, S. Vacuum Conveying in The Pharmaceutical Industry. *Pharmaceutical Technology Europe* **2010**, 22 (8), 1.
20. Hilbert, J. D. Pneumatic Points to Ponder. *Powder and Bulk Engin* **2019**, 18–21.
21. Pelletron. *The New Thinking in Pneumatic Conveying*; Bulk Inside: USA, 2018.
22. Leung, L. S.; Wiles, R. J.; Nicklin, D. J. Correlation for Predicting Choking Flowrates in Vertical Pneumatic Coveying. *Ind. eng. chem. process des. dev.* **1971**, 10 (2), 183–189.

23. How to Reduce Velocity and Prevent Buildup in Horizontal Pneumatic Conveying Lines. *Chemical Processing* **2005**, 1–2.
24. Ghadiri, M. Particle Impact Breakage. In *Powder Technology Handbook, Third Edition*; Masuda, H., Higashitani, K., Yoshida, H., Eds.; Taylor & Francis: London, England, 2006; pp 205–212.
25. US Naval Academy. Deformation. In *EN380: Naval Material Science and Engineering (3-0-3)*; US Naval Academy: Annapolis, Maryland; pp 1–10.
26. van Laarhoven, B. Breakage of Agglomerates, TU Delft, Delft, The Netherlands, 2010.
27. Kian-Pour, N.; Ozmen, D.; Toker, O. S. Modification of Food Powders. In *Food Powders Properties and Characterization*; Ermis, E., Ed.; Springer International Publishing: Cham, Switzerland, 2021; pp 125–154.
28. Elastic Properties of Materials – <https://www.lehman.cuny.edu/faculty/anchordoqui/chapter26.pdf> (accessed Jul 7, 2021).
29. Alderliesten, R. Material Types. In *Introduction to Aerospace Engineering – Structures and Materials*; Rene Alderliesten: Delft, The Netherlands, 2010; pp 37–53.
30. Valentini, L.; Lopez-Manchado, M. A. Classification of Rubbers and Components for Harsh Environmental Systems. In *High-Performance Elastomeric Materials Reinforced by Nano-Carbons: Multifunctional Properties and Industrial Applications*; Valentini, L., Lopez-Manchado, M. A., Eds.; Elsevier: London, Netherlands, 2020; pp 1–14.
31. Hanhi, K.; Poikelispää, M.; Tirilä, H.-M. *Elastomeric Materials*; Tampere University of Technology: Tampere, Finland, 2007.
32. Schawe, J. Applications Elastomers - Elastomers VKRT Bijeenkomst 8 Februari 2007 <https://vdocuments.net/applications-elastomers-elastomers-vkrt-bijeenkomst-8-februari-2007-hay-berden.html> (accessed Jul 7, 2021).
33. Eshel, G.; Levy, G. J.; Mingelgrin, U.; Singer, M. J. Critical Evaluation of the Use of Laser Diffraction for Particle-Size Distribution Analysis. *Soil Sci. Soc. Am. J.* **2004**, 68 (3), 736–743.
34. Barbosa-Canovas, G. V.; Ortega-Rivas, E.; Juliano, P.; Yan, H. *Food Powders: Physical Properties, Processing, and Functionality*; Springer: New York, NY, 2005.
35. Malvern Instruments Limited. *A Basic Guide to Particle Characterization*; 2015.
36. A basic guide to particle characterization <https://www.azom.com/article.aspx?ArticleID=12757> (accessed Jul 7, 2021).
37. Laser diffraction particle size analysis <https://www.malvernpanalytical.com/en/products/technology/light-scattering/laser-diffraction> (accessed Jul 7, 2021).
38. Hackley, V. A.; Lum, L.-S.; Gintautas, V.; Ferraris, C. F. *Particle Size Analysis by Laser Diffraction Spectrometry: Application to Cementitious Powders*; 2004.
39. Malvern Instruments Limited. *Morphologi G3 User Manual*; 2008.
40. Different sieving methods for varying applications <https://www.azom.com/article.aspx?ArticleID=14339> (accessed Jul 7, 2021).
41. Dhodapkar, S.; Solt, P.; Klinzing, G. Understanding Bends In Pneumatic Conveying Systems. *Chemical Engineering* **2009**, 53–60.
42. Transition and Turbulence [https://www.princeton.edu/~asmits/Bicycle\\_web/transition.html](https://www.princeton.edu/~asmits/Bicycle_web/transition.html) (accessed Jul 7, 2021).
43. Petit, J.; Michaux, F.; Jacquot, C.; Chávez Montes, E.; Dupas, J.; Girard, V.; Gianfrancesco, A.; Scher, J.; Gaiani, C. Storage-Induced Caking of Cocoa Powder. *J. Food Eng.* **2017**, 199, 42–53.
44. Tripathi, N. M.; Santo, N.; Kalman, H.; Levy, A. Experimental Analysis of Particle Velocity and Acceleration in Vertical Dilute Phase Pneumatic Conveying. *Powder Technol.* **2018**, 330, 239–251.

45. Wang, G.; Sun, S.; Zhang, Z. Randomness in Sequence Evolution Increases over Time. *PLoS One* **2016**, *11* (5), e0155935.
46. Borzone, L. A.; Klinzing, G. E.; Yang, W. C. Energy Losses and Particle—Wall Interactions on Rough Surfaces. *Powder Technol.* **1990**, *62* (3), 277–290.
47. Agarwal, A. T. Theory and Design of Dilute Phase Pneumatic Conveying Systems. *Powder Handling* **2005**, *17* (1), 18–23.
48. Specificities of vertical pneumatic conveying  
[https://www.powderprocess.net/Pneumatic\\_Transport/Vertical\\_Conveying.html](https://www.powderprocess.net/Pneumatic_Transport/Vertical_Conveying.html) (accessed Jul 7, 2021).
49. Choking Velocity in pneumatic transport - Correlation of Punwani - PowderProcess.net  
[https://powderprocess.net/Pneumatic\\_Transport/Choking\\_Velocity.html](https://powderprocess.net/Pneumatic_Transport/Choking_Velocity.html) (accessed Jul 7, 2021).
50. Kamel, A. H.; Shaqlaih, A. S. Frictional Pressure Losses of Fluids Flowing in Circular Conduits: A Review. *SPE Drill. Complet.* **2015**, *30* (02), 129–140.
51. Friction and Automobile Tires <http://hyperphysics.phy-astr.gsu.edu/hbase/Mechanics/frictire.html> (accessed Aug 1, 2021).

## Appendix

### Appendix 1

$$x_p^* = \frac{x_p}{[3(\mu_g)^2 + 4g\rho_g(\rho_s - \rho_g)]^{1/3}} \dots\dots\dots (\text{Eq. 2.4.1.1})$$

The parameter  $X_p^*$  is first calculated with Eq. 2.4.1.1.  $X_p$  is the particle size;  $\mu_g$  is the gas viscosity;  $\rho_g$  is the gas density;  $\rho_s$  is the particle density. If there is a mixture of particle sizes,  $X_p^*$  should be calculated for the largest and smallest particles. After obtaining  $X_p^*$ , Fig. 2.1.4.1 is read and  $U_{ss}^*$  is determined.

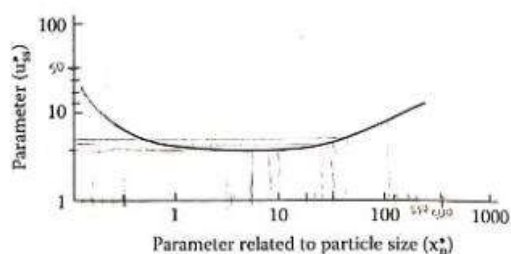


Fig. 2.1.4.1. Graph used to find  $U_{ss}^*$  after finding  $X_p^*$ .

With  $U_{ss}^*$ ,  $U_{ss}$  can be calculated with Eq. 2.4.1.2.

$$U_{ss} = 0.19(U_{ss}^*) \times \left[ \frac{4g\mu_g(\rho_s - \rho_g)}{3(\rho_g)^2} \right]^{1/3} \times (D_t)^{0.4} \dots\dots\dots (\text{Eq. 2.4.1.2})$$

With  $U_{ss}$ ,  $U_s$  (saltation velocity) can be calculated with the following Eq. 2.4.1.3 or 2.4.1.4 depending on the value of the slope of the graph in Fig. 2.1.4.1,  $n$ :

$$n = \frac{y_2 - y_1}{x_2 - x_1} = \frac{U_{ss2}^* - U_{ss1}^*}{(XP^*)_2 - (XP^*)_1} \dots\dots\dots (\text{Eq. 2.4.2.3})$$

If,

$n > 0.068$ , then,

$$\frac{G_s}{\rho_s} = \frac{0.214 (n)^{1.5} (U_s - U_{ss})}{U_{ss}} \dots\dots\dots (\text{Eq. 2.4.2.4})$$

And if  $-0.11 < n < 0.068$ , then,

$$\frac{G_s}{\rho_s} = \frac{0.0032 (U_s - U_{ss})}{U_{ss}} \dots\dots\dots (\text{Eq. 2.4.2.5})$$

To find  $U_s$ , Eqs. 2.4.2.4 and 2.4.2.5 were transposed.

Finally, to minimize the chances of the particles falling out of suspension, a safety factor of 10% is added to the saltation velocity, thus the initial air velocity is equal to the  $U_s + 10\% U_s$ .